

Contents lists available at ScienceDirect

## Petroleum Science

journal homepage: www.keaipublishing.com/en/journals/petroleum-science



Original Paper

## Enhance liquid nitrogen fracturing performance on hot dry rock by cyclic injection



Chun-Yang Hong <sup>a</sup>, Rui-Yue Yang <sup>a, \*</sup>, Zhong-Wei Huang <sup>a, \*\*</sup>, Xiao-Ying Zhuang <sup>b</sup>, Hai-Tao Wen <sup>a</sup>, Xiao-Li Hu <sup>a</sup>

- <sup>a</sup> State Key Laboratory of Petroleum Resources and Prospecting, China University of Petroleum, Beijing, 102249, China
- b Chair of Computational Science and Simulation Technology, Faculty of Mathematics and Physics, Leibniz Universität Hannover, Hannover, 30167, Germany

#### ARTICLE INFO

#### Article history: Received 11 February 2022 Received in revised form 15 July 2022 Accepted 17 July 2022 Available online 22 July 2022

Edited by Yan-Hua Sun

Keywords:
Hot dry rock
Liquid nitrogen fracturing
Cyclic injection
Thermal stress
Fatigue damage

#### ABSTRACT

Producing complex fracture networks in a safe way plays a critical role in the hot dry rock (HDR) geothermal energy exploitation. However, conventional hydraulic fracturing (HF) generally produces high breakdown pressure and results only in single main fracture morphology. Furthermore, HF has also other problems such as the increased risk of seismic events and consuption of large amount of water. In this work, a new stimulation method based on cyclic soft stimulation (CSS) and liquid nitrogen (LN<sub>2</sub>) fracturing, known as cyclic LN2 fracturing is explored, which we believe has the potential to solve the above issues related to HF. The fracturing performances including breakdown pressure and fracture morphology on granites under true-triaxial stresses are investigated and compared with cyclic water fracturing. Cryo-scanning electron microscopy (Cryo-SEM) tests and X-ray computed tomography (CT) scanning tests were used for quantitative characterization of fracture parameters and to evaluate the cyclic LN<sub>2</sub> fracturing performances. The results demonstrate that the cyclic LN<sub>2</sub> fracturing results in reduced breakdown pressure, with between 21% and 67% lower pressure compared with using cyclic water fracturing. Cyclic LN<sub>2</sub> fracturing tends to produce more complex and branched fractures, whereas cyclic water fracturing usually produces a single main fracture under a low number of cycles and pressure levels. Thermally-induced fractures mostly occur around the interfaces of different particles. This study shows the potential benefits of cyclic LN<sub>2</sub> fracturing on HDR. It is expected to provide theoretical guidance for the cyclic LN<sub>2</sub> fracturing application in HDR reservoirs.

© 2022 The Authors. Publishing services by Elsevier B.V. on behalf of KeAi Communications Co. Ltd. This is an open access article under the CC BY-NC-ND license (http://creativecommons.org/licenses/by-nc-nd/4.0/).

#### 1. Introduction

Recently, deep geothermal energy stored in hot dry rock (HDR) has gained increasing attention and has been recommended as an alternative clean and renewable energy resource (Lu, 2018; Song et al., 2021; Zhu et al., 2021). However, the heat energy is difficult to extract from the formation due to the low porosity, low permeability (0.001–0.1 mD) and deep burial depth of HDR reservoirs (Wang et al., 2021; Zhang et al., 2019). The building of an enhanced geothermal system (EGS) with fracture networks by hydraulic fracturing (HF) technology has provided the possibility of

E-mail addresses: yangruiyue@cup.edu.cn (R.-Y. Yang), huangzw@cup.edu.cn (Z.-W. Huang).

efficient heat energy extraction (Lv et al., 2022). As the most effective exploitation way of HDR reservoirs, the combination of HF technology and EGS has become the global hotspots, such as the Fenton Hill project in the USA (Kelkar et al., 2016), the Soultz project in France (Egert et al., 2020), Pohang project in South Korea (Kim et al., 2018), the Hijiori project in Japan (Tenma et al., 2008), etc. However, there are some critical issues in exploiting HDR energy by conventional HF technique. Firstly, the breakdown pressure can be very high in some formations due to the high strength of hard rock and high ground stress. During the stimulation period, the bottom hole pressure of the PX-2 well with 4348 m depths in the Pohang EGS site reached 131.8 MPa (Park et al., 2017). Secondly, single major fracture morphology is the common production by conventional HF in HDR reservoirs (Rahimi-Aghdam et al., 2019; Yang et al., 2021c). Creating complex fracture networks inside HDR is the key to improving the heat transfer efficiency between work

<sup>\*</sup> Corresponding author.

<sup>\*\*</sup> Corresponding author.

fluids and HDR reservoirs in EGS (Hofmann et al., 2014). Finally, the occurrence of induced or triggered seismic events during conventional HF treatment in EGS sites has raised wide public concern. The induced microseismicity reached  $M_{\rm W}$  5.5 in the Pohang EGS site (Kim et al., 2018). There are further examples of induced microseismicity such as  $M_{\rm L}$  3.7 (Baisch et al., 2006) and  $M_{\rm L}$  3.4 (Deichmann and Giardini, 2009) in the Cooper Basin EGS site and Basel EGS site during the stimulation period, respectively.

A new stimulation method, namely fatigue hydraulic fracturing (FHF) (Zang et al., 2013) or cyclic soft stimulation (CCS) (Hofmann et al., 2018), which applies varying innovative injection schemes, has been proposed to solve the above issues recently. The purpose of FHF or CCS is to inject fracturing fluids into HDR reservoirs by using alternating high-injection-rate and low-injection-rate under limited pressure, pressurization rates and net volumes to allow stress relaxation at the fracture tips (Zang et al., 2018). The recent laboratory experiments and field tests have investigated the performances of cyclic hydraulic fracturing in terms of breakdown pressure, fracture patterns, and the magnitudes of the induced seismic events (Patel et al., 2017; Zang et al., 2013; Zhuang et al., 2016, 2019; Zhuang and Zang, 2021). Their results indicated that induced seismicity by HF is expected to be relieved by cyclic injection due to the controlled release of crack-tip stresses according to Zhuang and Zang (2021). Besides, cyclic water injection can reduce the breakdown pressure and produce complex fracture networks with more branches and smaller apertures in comparison to conventional hydraulic fracturing (Patel et al., 2017; Zhuang et al., 2019). The reason behind is that damage accumulation and fatigue failure inside rocks during cyclic loading can lead to the decrease of local rock strength by generating an enlarged damage zone (Zang et al., 2018). Despite these advantages, CCS or FHF still has the issue of water consumption and waste-water disposal since large volumes of water needs to be injected into the reservoirs in order to create large heat-exchanging areas (EPA, 2016; Yoon et al., 2017).

A novel non-aqueous stimulation method in EGS development by using liquid nitrogen (LN<sub>2</sub>) as the fracturing fluid also has attracted more attention recently due to its unique advantages to fracture hard and high-temperature formations (Huang et al., 2020; Sun et al., 2022; Yang et al., 2019b, 2021c). At first, the temperature of LN<sub>2</sub> can reach -196 °C at atmospheric pressure (Wen et al., 2022). LN<sub>2</sub> fracturing can exert a large thermal gradient on nearborehole formations. This thermal shock can cause near-borehole shrink formations and create local tensile stress that will induce fractures (Cha et al., 2021). Micro-fractures orthogonal to the rock surface will be initiated when the tensile stress increases to a sufficiently high level (Wu et al., 2019). Moreover, LN2 can expand 694 times in volume at atmospheric pressure and room temperature (20 °C) (Yang et al., 2019a), which means newly thermally-induced fractures may extend even further by high-pressure nitrogen gas generated by LN<sub>2</sub> vaporization (Yang et al., 2021b). Cyclic LN<sub>2</sub> cooling treatment can further significantly deteriorate geomechanical properties such as compressive strength, tensile strength and elastic modulus, etc. (Rong et al., 2021; Wu et al., 2019), which benefits the formation of complex fracture pattern. The mechanical deterioration of rock can greatly decrease the breakdown pressure and facilitate the extension of main fractures and branches (Wu et al., 2019). Based on the above advantages, extensive laboratory and numerical studies have been conducted to explore the performance of LN<sub>2</sub> fracturing and its implications in the field, which can be divided into these three types: (a) cyclic heating and LN<sub>2</sub> cooling treatment before nitrogen-gas fracturing. It first generates micro-fractures inside rocks by take cyclic heating and LN<sub>2</sub> cooling treatment, and then nitrogen-gas is injected into rock to perform fracturing test (Yang et al., 2019b); (b) LN<sub>2</sub> assisted

nitrogen gas fracturing where low-pressure LN<sub>2</sub> is injected into the borehole to induced micro-fractures first, then nitrogen-gas injected afterwards to perform fracturing test (Cha et al., 2017, 2018; Wang et al., 2016); (c) high-pressure LN<sub>2</sub> fracturing which simply uses high-pressure LN<sub>2</sub> directly to perform fracturing test (Hong et al., 2022; Yang et al., 2021b, 2021c). The above methods have the potential to significantly decrease the breakdown pressure and produce more complex fracture networks inside rocks in comparison to conventional hydraulic fracturing technology. Despite these successes, to the best of the authors' knowledge there are only few published studies of the fracturing performance in HDR by cyclic LN<sub>2</sub> fracturing i.e. enhancing LN<sub>2</sub> fracturing performance by cyclic injection, especially under *in-situ* stresses. Hence, the fracturing performance and behaviour of cyclic LN<sub>2</sub> fracturing on high-temperature granites remain not understood.

To fill this research gap, the first controlled cyclic LN<sub>2</sub> fracturing tests on granites under *in-situ* stresses were conducted through laboratory experiments to explore the performance of cyclic LN<sub>2</sub> fracturing. Fracturing performances, including breakdown pressure and fracture morphology under various conditions, were studied. Cyclic water fracturing tests were also carried out as a comparison with cyclic LN<sub>2</sub> fracturing. Cryo-scanning electron microscopy (Cryo-SEM) tests and X-ray computed tomography (CT) scanning tests were used for quantitative assessment of fracture parameters and to reveal the cyclic LN<sub>2</sub> fracturing performances. It is expected to provide theoretical guidance for the cyclic LN<sub>2</sub> fracturing application in HDR reservoirs.

#### 2. Experimental equipment and experimental methods

## 2.1. Experimental materials

The schematic diagram of granite specimens taken cooling treatment by cyclic LN<sub>2</sub>/water injection can be found in Fig. 1 where

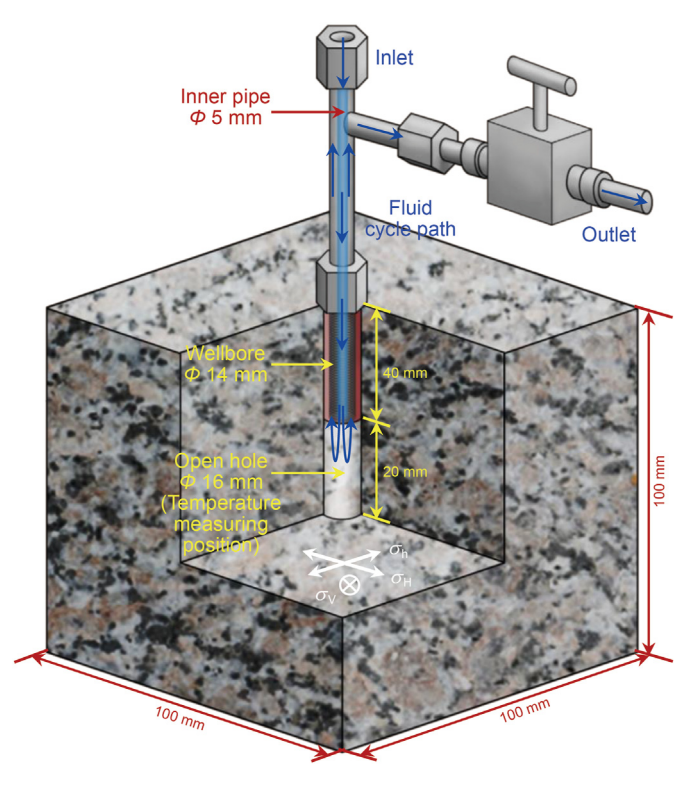


**Fig. 1.** Schematic diagram of granite specimens taken cooling treatment by cyclic LN<sub>2</sub>/ water injection.

 $\sigma_h$ ,  $\sigma_H$  and  $\sigma_V$  denote the minimum horizontal stress, maximum horizontal stress and vertical stress, respectively. The granite samples used in this study were taken from Shandong, China with the size of 100 mm  $\times$  100 mm  $\times$  100 mm. A 16-mm-diameter and 60-mm-depth borehole was drilled in the middle of a granite sample to represent scale-down wellbores before the fracturing experiment. A steel tubing with an outside diameter of 14 mm was placed inside the drilled hole and cemented using epoxy-resin adhesive. The casing extended 40 mm into the borehole with an open-hole section of 20 mm. A thermocouple attached to the open hole section was used to monitor the realtime temperature changes. Besides, granite specimens were cooling down by cyclic LN<sub>2</sub>/water injection under true triaxial stresses. LN<sub>2</sub> was injected into the wellbore through the inner pipe and discharged from the annulus between the inner pipe and wellbore for the cooling treatment of high-temperature granites. The hot nitrogen generated by contact with high-temperature granite can be discharged quickly to accelerate the cooling rate of the open hole section. The thermal shock inside high-temperature granite around the borehole was enhanced in this way. Water was injected into the wellbore through the inner pipe, but not discharged from the annulus to maintain the same injection pressure as the LN<sub>2</sub> injection. This is mainly because water injection cannot maintain the same injection pressure as LN2 injection when water is discharged from the annulus. The basic mechanical properties of granite is shown in Table 1.

#### 2.2. Experimental system

The true triaxial fracturing equipment which is shown in Fig. 2 consists of three systems, namely a true triaxial-loading system, a cyclic LN<sub>2</sub> injection system and a cyclic water injection system. The true triaxial-loading system (Fig. 2a) was designed to apply triaxial stress and heat preservation of granite specimens by the steel boards attached to a layer of asbestos insulation. The asbestos insulation was performed on a cuboid with a size of 400 mm  $\times$  400 mm  $\times$  10 mm. The thermal conductivity is 0.15–0.17 W/(m K) when the temperature is under 1000  $^{\circ}\text{C}.$  It has excellent thermal insulation, high compressive strength and good frost resistance to ensure the normal operation of hightemperature granite fracturing experiments. An outer circle and an inner square structure were adopted in the kettle body. The can capacitate the specimen size  $400 \text{ mm} \times 400 \text{ mm} \times 400 \text{ mm}$  and pressure up to 50 MPa. Water can be injected into the boreholes at constant flow rate mode or constant pressure mode by using the cyclic water injection system (Fig. 2b). The water was injected into the boreholes at a constant flow rate when in constant flow rate mode. In constant pressure mode, the water was injected at the set flow rate first. Once the injection pressure reached the set value, the injecting was stoped to maintain the pressure. Once the injection pressure was lower than

**Table 1**Basic mechanical properties of the granite.

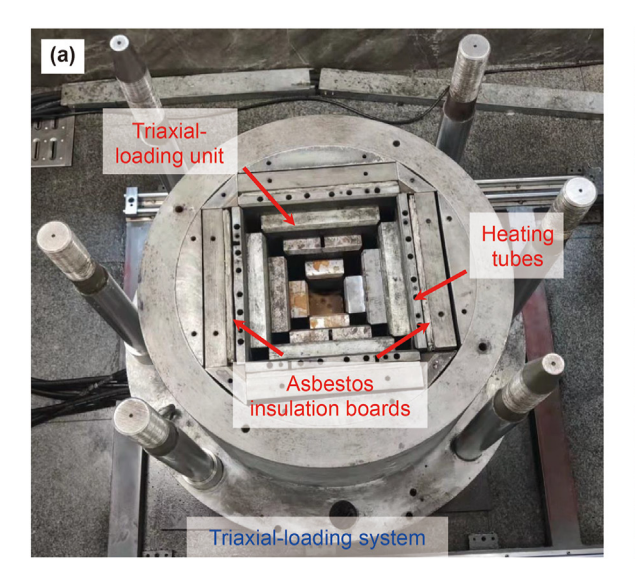
Properties	Value
Density, kg/m <sup>3</sup>	2630
Uniaxial compressive strength, MPa	121.97
Tensile strength, MPa	10.02
Young's modulus, GPa	39.41
Poisson's ratio	0.28
Permeability, mD	$11.60 \times 10^{-3}$
Porosity, %	0.45
Cohesive strength, MPa	44.84
Internal friction angle, degree	48.74

the set value, the water was injected into the borehole at the set flow rate to maintain the pressure. The maximum injection pressure of the cyclic water injection system can reach 100.0 MPa. The maximum flow rate and maximum volume of a single injection were 100.0 mm<sup>3</sup>/min and 800 mm<sup>3</sup> with an accuracy of  $\pm 0.1$  mm<sup>3</sup>/ min. respectively. Considering the ultra-low temperature of LN<sub>2</sub>, the conventional injection pump is difficult to meet the experimental requirements, which brings many problems such as piston freezing easily, adding LN2 difficulty and sealing element failure during LN<sub>2</sub> injection. Therefore, high-pressure nitrogen gas was used to push the ultra-low temperature LN2 into the borehole to perform the high-pressure LN<sub>2</sub> fracturing test in this study. The cyclic LN<sub>2</sub> injection system was designed to produce low-pressure LN<sub>2</sub> for the cooling of high-temperature granite specimens and inject high-pressure LN<sub>2</sub> into the boreholes to simulate the fracturing process. The cyclic LN<sub>2</sub> injection system consists of four devices including a self-pressurization LN<sub>2</sub> tank, a high-pressure LN<sub>2</sub> container, a gas pressurizer and an air compressor, as shown in Fig. 2c. LN<sub>2</sub> was stored in the self-pressurization LN<sub>2</sub> tank at first. Then, LN<sub>2</sub> flowed from the self-pressurization tank along the green arrows, which is pushed by the nitrogen gas generated inside the self-pressurization LN<sub>2</sub> tank, to fill the high-pressure LN<sub>2</sub> container. The nitrogen-gas pressure inside the LN<sub>2</sub> self-pressurization tank can be adjusted between 1 and 3 MPa as shown in Fig. 3. The hightemperature granite specimens were cooled down by the lowpressure LN<sub>2</sub> from the self-pressurization LN<sub>2</sub> tank and this process can be repeated after the granite specimens were reheated. Finally, the high-pressure nitrogen-gas generated by the gas pressurizer flows into a high-pressure LN2 container along the red arrows in Fig. 3 and pushed LN<sub>2</sub> into the boreholes along the blue arrows to perform the high-pressure LN<sub>2</sub> fracturing test. The maximum volumes of self-pressurized LN<sub>2</sub> tank and high-pressure LN<sub>2</sub> container were 175 and 5 L, respectively. The maximum pressures of self-pressurized LN<sub>2</sub> tank and high-pressure LN<sub>2</sub> container were 4 and 30 MPa, respectively. Thermal insulation materials were applied outside the pipelines to maintain LN<sub>2</sub> at its cryogenic state during the cyclic injection. The details of this cyclic LN<sub>2</sub> injection system can be seen in our previous works (Huang et al., 2019; Yang et al., 2021c).

#### 2.3. Experimental procedure and matrix

The cyclic LN<sub>2</sub>/water fracturing performance of granite specimens was tested under various conditions in this study. For each granite specimen fracturing by cyclic LN<sub>2</sub> injection, the experimental procedures generally followed the following steps:

- (1) Pre-heat the granite specimen in a muffle furnace to 200 °C. Then load the granite specimens to the set value of *in-situ* stresses (stage I in Fig. 5c in Section 3.1).
- (2) Before injecting high-pressure LN<sub>2</sub> to perform the fracturing test, inject LN<sub>2</sub> at low-pressure levels within 1–3 MPa to precool the pipelines and boreholes until it is discharged from the annulus between the inner pipe and wellbore as shown in Section 3.1 (stage II in Fig. 5d).
- (3) Take out the granite specimen from the true triaxial-loading unit. Then put the specimen in the muffle furnace to 200 °C again and one cooling treatment cycle is finished (stage III in Fig. 5e).
- (4) Repeat steps (1), (2) and (3) to make cooling treatment cycles reach the target value and then put on to fracturing test.
- (5) Fill the high-pressure LN<sub>2</sub> container with low-pressure LN<sub>2</sub> which is transported from the self-pressurization LN<sub>2</sub> tank. Boost the low-pressure nitrogen gas from the nitrogen gas













Cyclic LN<sub>2</sub> injection system

Fig. 2. True triaxial fracturing equipment for the formation temperatures and pressures. (a) True triaxial-loading system; (b) Cyclic water injection system; (c) Cyclic LN<sub>2</sub> injection system.

- tank to high-pressure nitrogen gas (30–45 MPa) by the gas pressurizer, simultaneously.
- (6) Repeat step (2) to cool down the pipelines and boreholes to make sure the later injected high-pressure  $LN_2$  maintains ultra-low temperature. This is the last cooling treatment cycle.
- (7) Open the reducing valves to allow the high-pressure nitrogen gas to push the LN<sub>2</sub> inside high-pressure LN<sub>2</sub> container into the borehole to accomplish a high-pressure cyclic LN<sub>2</sub> fracturing test. The pressure and temperature data should be recorded during the entire injection process (stage IV in Fig. 5f).

In cyclic water fracturing, the water was injected into the boreholes directly. During the low-pressure water injection stage (stage II in Fig. 5d), the pump was in the constant pressure mode. It injected water into the boreholes at a constant flow rate of 30 mm<sup>3</sup>/min first. Once the pressure reached the set value of cooling treatment pressure, the injection was stoped. Meanwhile, the pump started to work automatically to maintain the wellbore pressure at the set value when the pressure dropped. During the high-pressure water injection stage (stage IV in Fig. 5f), the injection pump was in constant flow mode with a constant injection-

flow rate of 30 mm<sup>3</sup>/min.

The average pressurization rate (dP/dt) of cyclic LN<sub>2</sub>/water fracturing tests were 0.388 and 0.386 MPa/s, respectively. The experimental parameter setting of cyclic LN<sub>2</sub>/water fracturing tests in this study is listed in Table 2. 18 specimens were used for fracturing tests under various fracturing fluids, cooling treatment pressure, cooling treatment time and cooling treatment cycles. The in-situ stress data of the HDR reservoirs from the FORGE site in the USA showed that the horizontal stress difference ratio (( $\sigma_H$  –  $\sigma_h$ )/ $\sigma_h$ ) is within the range of 0.1–0.4 (EGI, 2018). For well GR1 in Gonghe Basion, the horizontal stress difference ratio is about 0.1–0.4 and the average temperature of the HDR is 218 °C (Lei et al., 2019). Hence, in this study the horizontal stress difference ratio and specimen initial temperature were set 0.4  $(\sigma_{\rm H}/\sigma_{\rm h}/\sigma_{\rm V}=10.0/7.0/15.0$  MPa) and 200 °C, respectively.

#### 2.4. Fracture identification and fracture conductivity calculation

After the fracturing test, induced fractures were colored by injecting dye solution into the borehole at a constant injection-flow rate of 30 mm<sup>3</sup>/min without any confining stress to identify the fracture distributions. The reinjection pressure eventually stabilized at a certain value which can be indicated by the dye solution

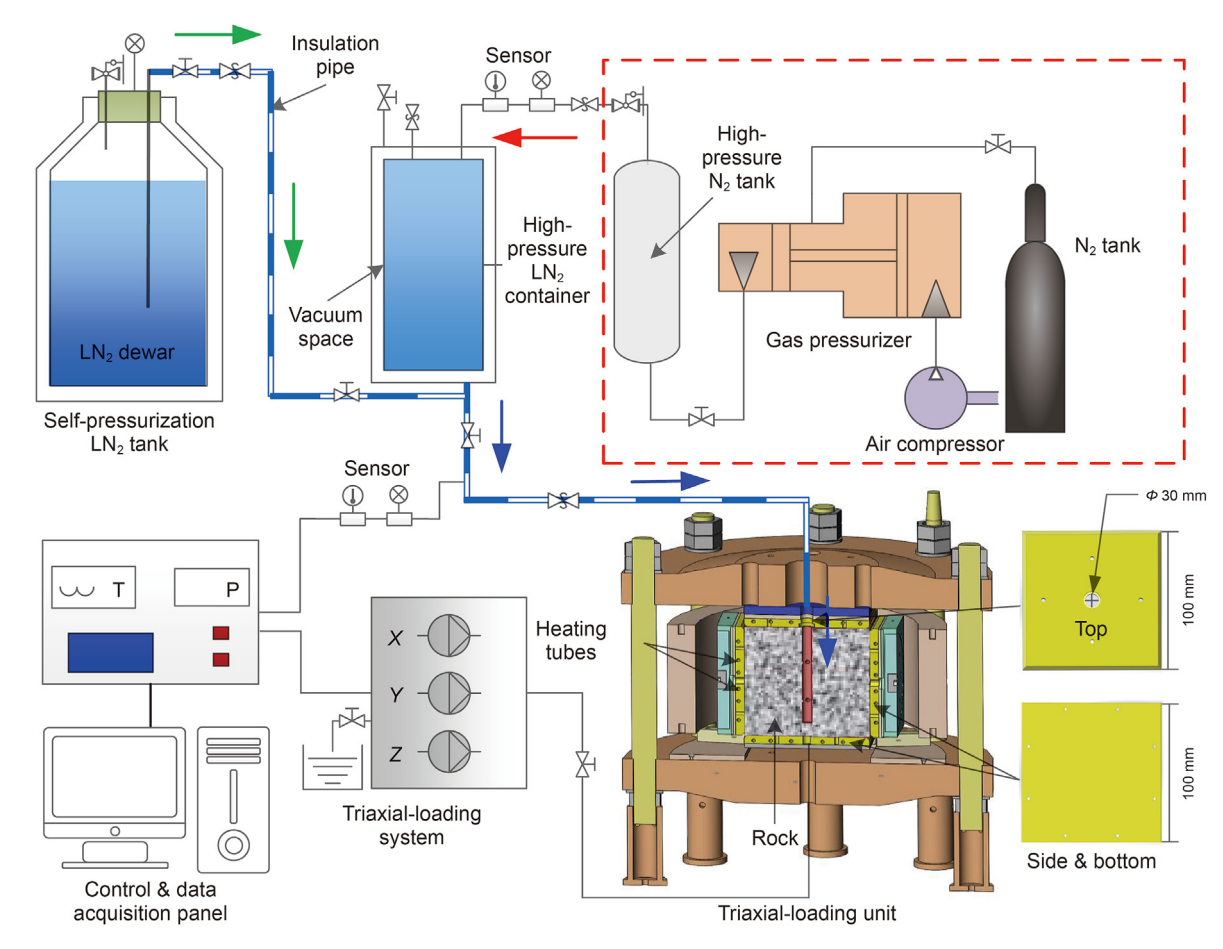


Fig. 3. Schematic of the true triaxial cyclic LN<sub>2</sub> fracturing equipment. Green arrows show low-pressure LN<sub>2</sub> transport route; red arrows show high-pressure nitrogen-gas transport route; blue arrows show LN<sub>2</sub> injection route (Yang et al., 2021c).

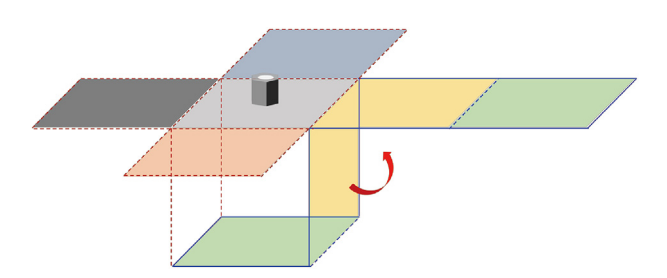


Fig. 4. Schematic that shows the intact fracture morphology of a specimen.

that migrated to the surface by a steady seepage along with the induced fractures. The stabilized reinjection pressure can be used to calculate the fracture conductivity. A detailed description of the calculation method can be found in our previous work (Yang et al., 2021b), which can be expressed as

$$C_{\rm f} = \frac{25q_{\rm w}\mu\,\ln\left(\frac{r_{\rm e}}{r_{\rm w}}\right)}{3\pi\Delta P_{\rm wf}},\tag{1}$$

where  $C_{\rm f}$  represents the fracture conductivity, mD mm;  $r_{\rm e}$  represents the effective radius, mm;  $r_{\rm w}$  represents the wellbore radius, mm;  $q_{\rm w}$  represents the flow rate, mm<sup>3</sup>/min;  $\mu$  represents the reinjected-water viscosity, mPa s;  $\Delta P_{\rm wf}$  represents the reinjection pressure, MPa.

Then, the location of induced fractures on the surface of the

specimen can be marked simultaneously. The intact fracture morphology of a specimen can be displayed at the same time by the method as shown in Fig. 4.

## 2.5. CT scanning and Cryo-SEM imaging

To obtain the fracture morphology inside the specimens, CT scanning is usually used after fracturing tests (Li et al., 2022). CT scanning provides a reliable quantitative analysis of induced fractures inside granite samples and in this study the CT has a resolution of 40  $\mu m \times 40~\mu m \times 40~\mu m$ . The aperture, length, tortuosity, deviation angle, surface area and volume of induced fractures were obtained based on 3D reconstruction of fracture morphology. The length is the total length of fractures in each 2D CT image. According to previous work, the tortuosity can be estimated by (Hou et al., 2018):

$$C = \frac{L}{L_{\rm d}},\tag{2}$$

where  $\it C$  represents the fracture tortuosity;  $\it L$  and  $\it L_d$  represent the direct length and the cumulative length between the two ends of a fracture, respectively.

Besides, the deviation angle can be calculated by (Yang et al., 2021a):

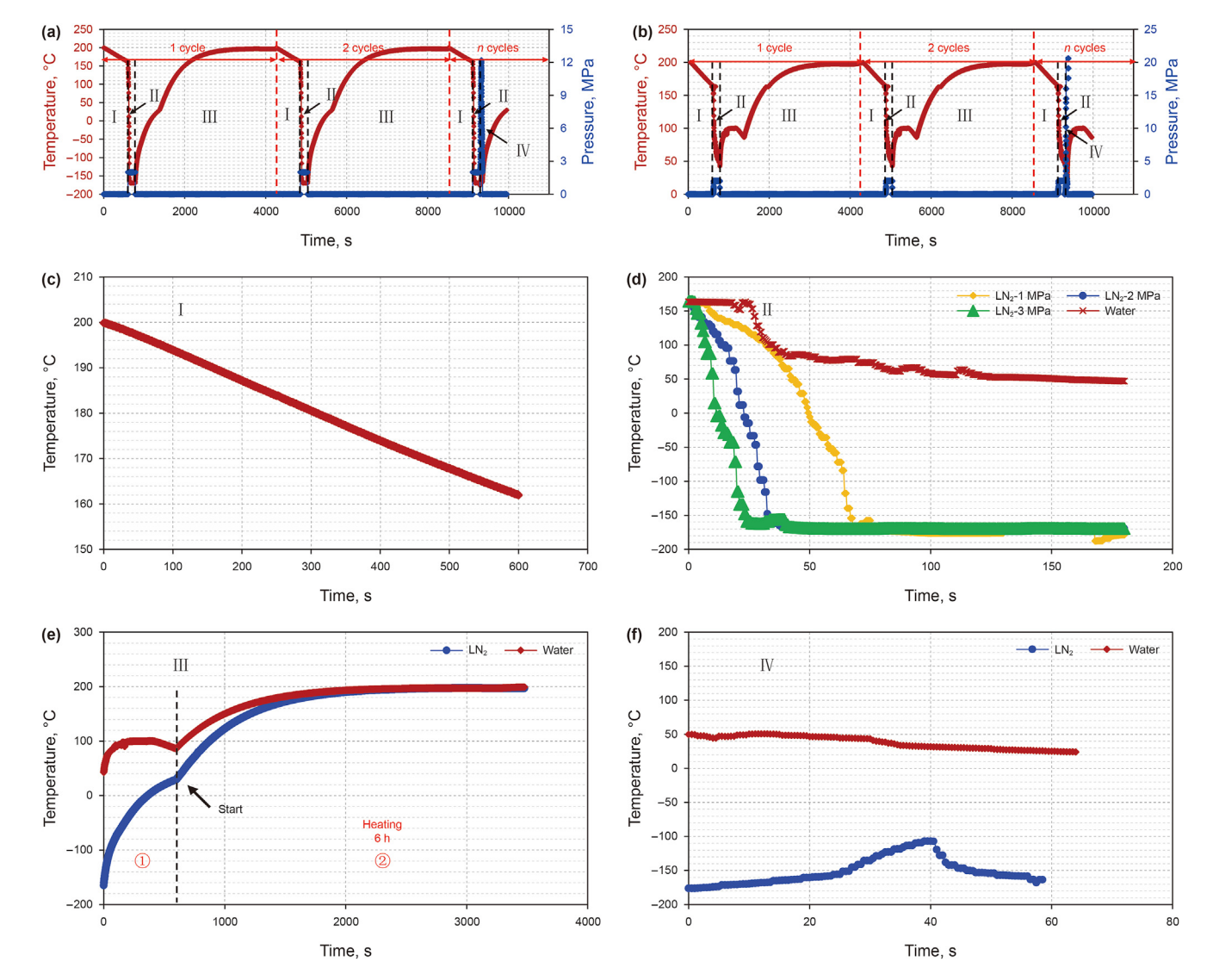


**Fig. 5.** Temperature and pressure alternation curves during cyclic LN<sub>2</sub> and water injection. Temperature and pressure alternation curves during (**a**) cyclic LN<sub>2</sub> injection and (**b**) cyclic water injection. (**c**) Stage II: temperature natural decline curves before fracturing fluid injection; (**d**) Stage II: temperature curves during low-pressure LN<sub>2</sub> and water injection for cyclic cooling treatment; (**e**) Stage III: temperature curves during high-pressure LN<sub>2</sub> and water injection for fracturing.

**Table 2** Experimental matrix for cyclic LN<sub>2</sub> and water injection on each granite specimen.

Specimen No.	Fracturing fluid	Cooling treatment pressure, MPa	Cooling treatment time, s	Number of cycles	Breakdown pressure, MPa	Reinjection pressure, MPa
LN1	LN <sub>2</sub>	1	180	3	16.6	0.78
LN2	$LN_2$	2	180	3	10.5	0.58
LN3	$LN_2$	3	180	3	6.8	0.18
LN4	$LN_2$	2	60	3	16.7	0.39
LN5	$LN_2$	2	300	3	8.1	0.56
LN6	LN <sub>2</sub>	2	600	3	7.5	0.36
LN7	LN <sub>2</sub>	0	0	0	26.7	1.62
LN8	LN <sub>2</sub>	2	180	1	18.1	0.26
LN9	LN <sub>2</sub>	2	180	5	5.9	0.46
W1	Water	1	180	3	21.1	3.56
W2	Water	2	180	3	19.8	4.63
W3	Water	3	180	3	20.7	3.65
W4	Water	2	60	3	22.9	2.96
W5	Water	2	300	3	17.8	3.59
W6	Water	2	600	3	19.0	3.78
W7	Water	0	0	0	24.7	2.89
W8	Water	2	180	1	23.1	3.56
W9	Water	2	180	5	13.7	2.68

$$\theta = \cos^{-1} \left( \frac{\mathbf{n}_{\mathbf{f}} \cdot \mathbf{n}_{\mathbf{p}}}{|\mathbf{n}_{\mathbf{f}}| \cdot |\mathbf{n}_{\mathbf{p}}|} \right) \tag{3}$$

where  $\theta$  represents the deviation angle;  $\mathbf{n}_{p}$  and  $\mathbf{n}_{f}$  represent the direction of the maximum horizontal stress and the normal vector of fracture plane in this study, respectively.

To investigate the thermal shock induced fractures on hightemperature granite by LN<sub>2</sub>, Cryo-SEM analysis was conducted to examine the in-situ fracture patterns and to quantify the fracture sizes that resulted from LN<sub>2</sub> cooling treatment. Direct observation of induced fractures by alternating thermal stress at cryogenic conditions (-190 °C) is critical to improve our understanding of the cyclic LN2 fracturing mechanism on HDR reservoirs. To make a comparison with the state after cyclic LN<sub>2</sub> cooling treatment, the specimen with the size of 10 mm  $\times$  5 mm  $\times$  2 mm was scanned at room temperature at first. Besides, the surface morphology and mineral distribution were measured by using a mineral analysis system with a resolution of 0.39  $\mu m \times$  0.39  $\mu m$ . Then, the specimen was frozen in LN<sub>2</sub> for at least 10 min after being heated to 200 °C in a metal bath for more than 20 min. Micro-fractures were initiated by thermal shock during the period of the cyclic heating and LN<sub>2</sub> cooling treatment. After observation by Cryo-SEM under cryogenic conditions, the specimen was turned into the next heating and freezing cycle. The procedure of Cryo-SEM observation can be found in our previous work (Yang et al., 2021c).

#### 3. Experimental results

#### 3.1. Temperature and pressure during cyclic LN<sub>2</sub>/water injection

The temperature and pressure of boreholes during cyclic LN<sub>2</sub>/ water injection were presented in Fig. 5. In stage I, true triaxial stresses were loaded to the specimen. The borehole temperature naturally declined from 200 °C to around 160 °C in 600 s simultaneous. In stage II, low-pressure LN<sub>2</sub>/water was injected into the borehole for the cyclic cooling treatment of specimens. The cooling rate of LN<sub>2</sub> was significantly higher as compared to that with water. Also the cooling rate was higher at the high cooling treatment pressure. When the cooling treatment pressures were 1, 2 and 3 MPa, the cooling rate presented were around 5, 9 and 13 °C/s, respectively. Under the low-pressure injection, the temperature of boreholes by water injection was decreased to about 50 °C slowly after 180 s. As a comparison, the terminal temperature by LN2 injection was maintained between −165 and −175 °C. However, LN<sub>2</sub> can reach -196 °C at atmospheric pressure (boiling point). This is mainly because the phase boundary and boiling point of nitrogen are affected by the pressure (Cha et al., 2021). The boiling point of nitrogen rises with pressure generally. The temperature inside the specimen remained high and also depended on their proximity to the thermally-induced fractures. In stage III, the temperature of boreholes increased gradually (stage 1): remove the specimen without muffle furnace heating; stage ②: muffle furnace heating). During the cyclic LN<sub>2</sub>/water injection and heating, an alternation huge thermal gradient was created between the borehole and the inside specimen. In stage IV, high-pressure LN2 and water were injected into the boreholes for fracturing. The temperature of boreholes by water injection was decreased to about 30 °C slowly during fracturing tests. However, the temperature of boreholes by LN<sub>2</sub> injection was increased to around -100 °C and then decreased to about -170 °C slowly. The possible reason is that the outlet as shown in Fig. 1 was closed when injected with the high-pressure LN<sub>2</sub>. The borehole temperature gradually increased due to the heat flow from the specimen. Then, the heated nitrogen leaked

from the fractures and the cold  $LN_2$  entered the borehole once the specimen was fractured so that the temperature gradually decreased.

#### 3.2. Effect of cooling treatment pressure

The pressure—time curves and breakdown pressures of cyclic LN<sub>2</sub>/water fracturing tests on granite specimens under various cooling treatment pressures were shown in Fig. 6. It should be noted that the pressure in the high-pressure LN<sub>2</sub> container (Fig. 2c) will increase gradually resulting from the volume expansion of nitrogen under room temperature (20 °C), which leads to the pressure-time curves of LN<sub>2</sub> fracturing tests starting at relatively higher pressure. Then, it can be seen that cyclic LN<sub>2</sub> fracturing represents lower breakdown pressure in comparison to cyclic water fracturing. Under the same cooling treatment time and cycle number, cyclic LN<sub>2</sub> fracturing presented 21.3%, 47.0% and 67.2% lower breakdown pressure than cyclic water fracturing, respectively, when the cooling treatment pressure increased from 1 to 3 MPa. It indicated that cyclic LN<sub>2</sub> fracturing shows the potential to decrease more breakdown pressure when specimens are cooled by higher injection pressure. A higher injection pressure/rate allows for better thermal exchange and a more depressed thickness of contact film boiling (the Leidenfrost effect (Li et al., 2018)), which facilitates thermal conduction and enhances the cooling rate (Cha et al., 2021; Li et al., 2019). A higher cooling rate is favorable for thermal shock and enhances the thermal shock because it creates larger local thermal gradients according to Fig. 5d. The thermallyinduced fractures around the boreholes could facilitate the initiation of major fractures (Yang et al., 2021c). Besides, the tensile stress induced by the LN<sub>2</sub> injection and thermal stress induced by thermal shock is superimposed on each other, which leads to cyclic LN<sub>2</sub> fracturing being more favorable to reaching the breakdown condition (Zhang et al., 2018). Moreover, LN<sub>2</sub> has a strong penetrating capacity (lower viscosity and low interfacial tension), which makes it effortless to flow through the rock matrix and micro-pores/ fractures in comparison to water. The developed pore pressure distribution by LN<sub>2</sub> injection not only induces circumferential stress around the borehole but also weakens the strength of specimens (Hou et al., 2018). As a comparison, increased cooling treatment pressure of cyclic water fracturing had no contribution to reducing the breakdown pressure basically due to the poor thermal shock induced by water injection in this study. However, it is worth noting that the performance of cyclic water fracturing can be greatly improved by increasing the number of cycles and cooling treatment pressure (Hofmann et al., 2018; Patel et al., 2017; Zang et al., 2021; Zhuang et al., 2019, 2020). In this study, the performance of cyclic water fracturing is mainly used to compare with the cyclic LN<sub>2</sub> fracturing. Hence, the number of cycles and pressure level during cyclic injection in this study was too low to increase relatively large-scale fatigue damage around boreholes compared with previous works.

The fracture morphology under various cooling treatment pressures was presented in Fig. 7. It can be found that cyclic  $LN_2$  fracturing shows the potential to lead to complex fracture networks rather than a single main fracture in comparison to cyclic water fracturing. Besides, the fracture patterns become branched with increasing cooling treatment pressure and form complex fracture networks when the cooling treatment pressure reached 3 MPa. However, increased cooling treatment pressure of cyclic water fracturing had no contribution to enhancing the fracture complexity in this study either. This can be attributed to a huge number of micro thermally-induced fractures that were induced around the boreholes by cyclic  $LN_2$  cooling treatment, which facilitates the propagation of complex fracture networks (Cha et al.,

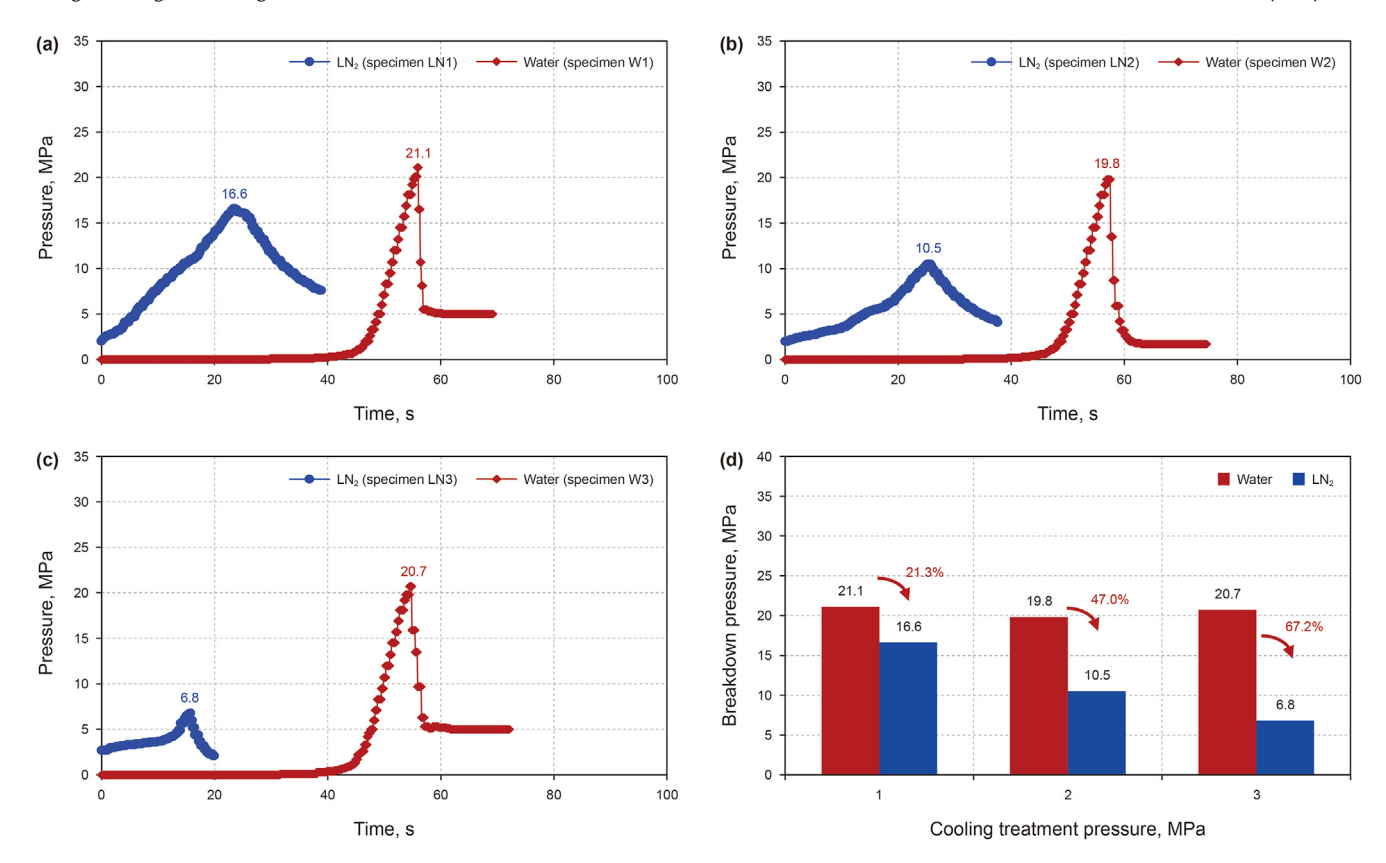


**Fig. 6.** Pressure—time curves under various cooling treatment pressures ( $P_c$ ) (**a**)  $P_c = 1$  MPa, (**b**)  $P_c = 2$  MPa, and (**c**)  $P_c = 3$  MPa; (**d**) Comparison of breakdown pressure between cyclic LN<sub>2</sub> fracturing and cyclic water fracturing under various cooling treatment pressures. Other experimental parameters are as follows: the cooling treatment time  $t_c$  is 180 s, and the number of cycles n is 3.

2018). Borehole pressurization can enhance the thermal-induced damage by applying a level of pressure to the borehole (Cha et al., 2014). Moreover, the volume of  $LN_2$  will expand rapidly when in contact with high-temperature granites, which could facilitate the propagation of induced fractures.

#### 3.3. Effect of cooling treatment time

Pressure—time curves under various cooling treatment pressures were compared in Fig. 8. It can be found that cyclic LN<sub>2</sub> fracturing presented 27.1%, 47.0%, 54.5% and 60.5% lower breakdown pressure in comparison to cyclic water fracturing, respectively under the same cooling treatment pressure and the number of cycles when the cooling treatment times were 60, 180, 300 and 600 s, respectively. It indicated that cyclic LN<sub>2</sub> fracturing shows the potential to reduce more breakdown pressure when specimens are taken longer cooling treatment. However, the breakdown pressure of cyclic water fracturing decreased slightly when the cooling treatment times increased from 60 to 600 s. The range of thermal shock regions increased gradually and the breakdown pressure level of the reservoir rocks can be reduced.

Fracture patterns under various cooling treatment times were presented in Fig. 9. It can be concluded that the complexity of fractures by cyclic  $LN_2$  fracturing was increased obviously with the cooling treatment time increased from 60 to 180 s but increased gradually with the cooling treatment time increased from 180 to 300 s. However, it showed no significant change in cyclic water fracturing with the increment of cooling treatment time. The decreasing amplitude of breakdown pressure by cyclic  $LN_2$  fracturing gradually decreased with the increase in cooling down

pressure as shown in Fig. 8e. It was 6.2, 2.4 and 0.6 MPa when the cooling treatment time decreased from 60 to 180 s, from 180 to 300 s, and from 300 to 600 s. It indicated that SRV (stimulated reservoir volume) and breakdown pressure of hot dry rock reservoirs fractured by cyclic  $LN_2$  injection can be improved significantly by increasing cooling treatment time within a certain range. As explained above, although no breakdown was observed from the pressure-time curves, damage (e.g., micro thermally-induced fractures) may have already accumulated within the specimen during cyclic  $LN_2$  injection. This may also account for the subsequent breakdown pressure being smaller and for the greater complexity of the fractures than cyclic water injection.

However, simply increasing cooling treatment time may not be beneficial when considering the economic conditions and the actual situation on the site. Besides, we know that as the well depth increases, the temperature of LN<sub>2</sub> tends to rise as it is transported along the string to the boreholes, which makes it difficult to reach the cooling rate presented in this study (Fig. 5). The cyclic fracturing performance will be greatly affected. According to the previous works, increasing the number of cycles (heating and cooling cycles) can effectively improve both the level and region of thermal shock (Feng et al., 2020; Li et al., 2021; Pai et al., 2021; Zhu et al., 2021). Hence, we also explore the effect of the number of cycles on LN<sub>2</sub> fracturing performance.

#### 3.4. Effect of number of cycles

Pressure—time curves under various cycles can be found in Fig. 10. It can be concluded that both the breakdown pressure of cyclic  $LN_2$  and water fracturing decreased significantly with the

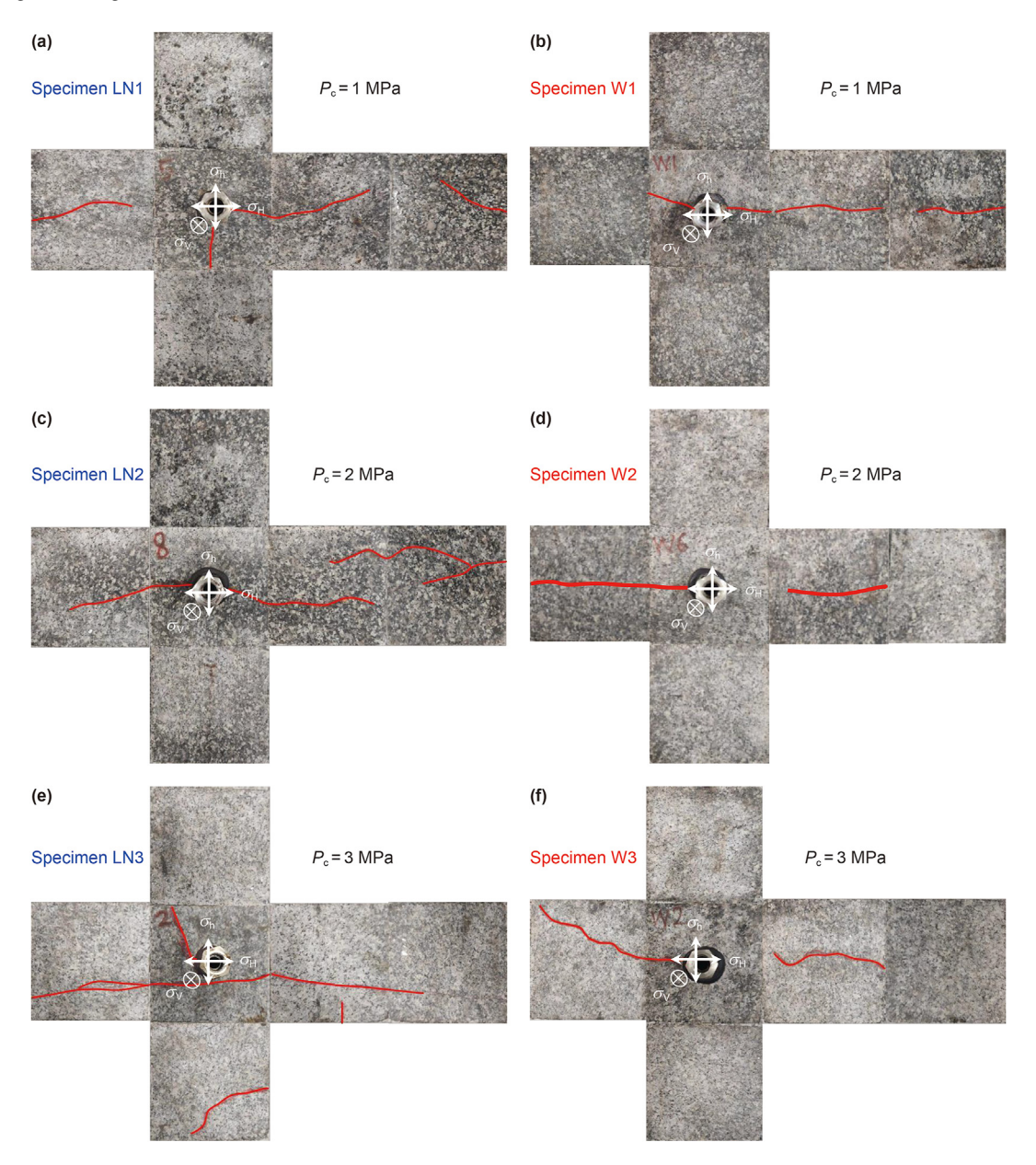


**Fig. 7.** Fracture patterns induced by cyclic LN<sub>2</sub> fracturing (**a**, **c**, **e**) and cyclic water fracturing (**b**, **d**, **f**) under various cooling treatment pressures (*P*<sub>c</sub>). Red solid lines show the induced fractures.

increase in the number of cycles. Cyclic LN<sub>2</sub> fracturing presented 21.6%, 47.0%, and 56.9% lower breakdown pressure in comparison to cyclic water fracturing when the numbers of cycles were 1, 3 and 5, respectively. It indicated that the cooling-heating cycles are conducive to enhancing the thermal shock around the boreholes. Thermal shock in each injection cycle was generated despite total macro-failure not being achieved. During the cyclic low-pressure LN<sub>2</sub> and water injection stage, the localized thermal fatigue damage was induced by the coupled hydraulic-thermal stress. New fractures were constantly generated to communicate with the existing pores and fractures. The fracturing width of localized region also increased with the number of cycles as discussed in Section 4.2. The permeability, uniaxial compressive strength, elastic modulus, tensile strength and fracture toughness of granite specimens can be decreased simultaneously according to Wu et al. (2019) and Rong et al. (2021), which also facilitated the reduced breakdown pressure. A reduction in breakdown pressure has the

benefit of reducing the energy inputs and possibly mitigating earthquakes. However, cyclic  $LN_2$  fracturing presented 8.1% higher breakdown pressure compared with cyclic water fracturing when the cycle time was 0 (without cooling treatment). The main reason is that when the high-pressure  $LN_2$  is injected into the boreholes directly, the  $LN_2$  vaporizes rapidly in contact with the high-temperature specimen. The hot nitrogen cannot be discharged, resulting in a lower cooling rate and difficulty in forming strong thermal shock around boreholes. It was similar to conclusion of the high flow rate of nitrogen-gas fracturing found in our previous works (Yang et al., 2021c).

Fracture patterns under various cycles were presented in Fig. 11. It can be found that cyclic  $LN_2$  fracturing shows the potential to lead to 3D volumetric patterns that consist of major fractures and fracture patterns with branches while cyclic water fracturing can only lead to a bi-wing fracture along with the direction of maximum horizontal stress. Besides, the total lengths and complexity of

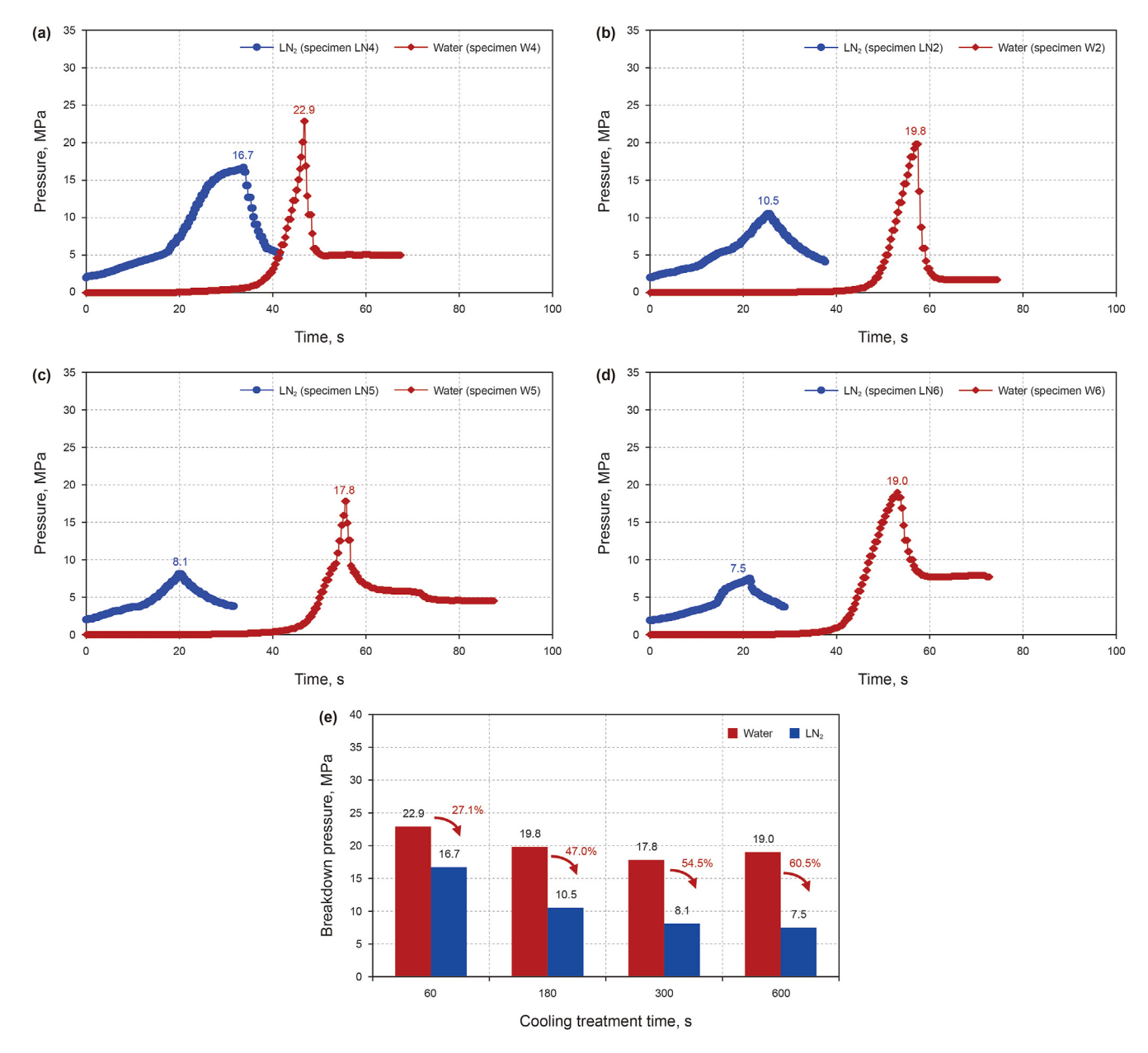


**Fig. 8.** Pressure—time curves under various cooling treatment times: (**a**)  $t_c = 60$  s, (**b**)  $t_c = 180$  s, (**c**)  $t_c = 300$  s, (**d**)  $t_c = 600$  s; (**e**) Comparison of breakdown pressure between cyclic LN<sub>2</sub> fracturing and cyclic water fracturing under various treatment times. Other experimental parameters are as follows: the cooling treatment pressure  $P_c$  is 2 MPa, and number of cycles n is 3.

induced fractures by cyclic LN<sub>2</sub> fracturing were significantly increased with the number of cycles while it showed no significant change by cyclic water fracturing. It indicated that the cyclic LN<sub>2</sub> fracturing shows the potential to form complex fracture networks with higher conductivity and larger scale. Hence, cryogenic fracturing performance on hot dry rock can be enhanced significantly by cyclic LN<sub>2</sub> injection compared with a single LN<sub>2</sub> injection or cyclic water injection. However, increasing the number of cycles does not mean it is always better in the field application. According to the previous works, the damage of granite under cyclic heating and LN2 cooling treatment mainly occurs within the initial few cycles. However, the mechanical properties decreased smaller with the increase in the number of cycles after about 10 cycles (Wu et al., 2019). Hence, the stimulation performance and engineering cost should be considered together to optimize the number of cycles in the field application.

# 3.5. 3D reconstruction and quantitative analysis of induced fractures

To provide a comprehensive quantitative analysis of the fracture morphology inside the specimens as shown in Sections 3.2, 3.3 and 3.4, three representative samples (Nos. W2, LN2 and LN9) were chosen for the CT scanning after cyclic LN2/water fracturing tests. Firstly, typical 2D CT images were presented in Fig. 12a. Then, 3D reconstruction of fracture patterns was presented in Fig. 12b. Note that some micro-fractures smaller than the image resolution of 40  $\mu m$  per pixel may have been omitted. Since fractures exist in three dimensions, their performance and locations vary in various cross-sections through the specimens. Hence, some major fractures and fracture branches initiated from the borehole throughout to the specimen surface presented in Section 3 haven't been shown in the 2D CT image and 3D reconstruction due to the restricted resolution.

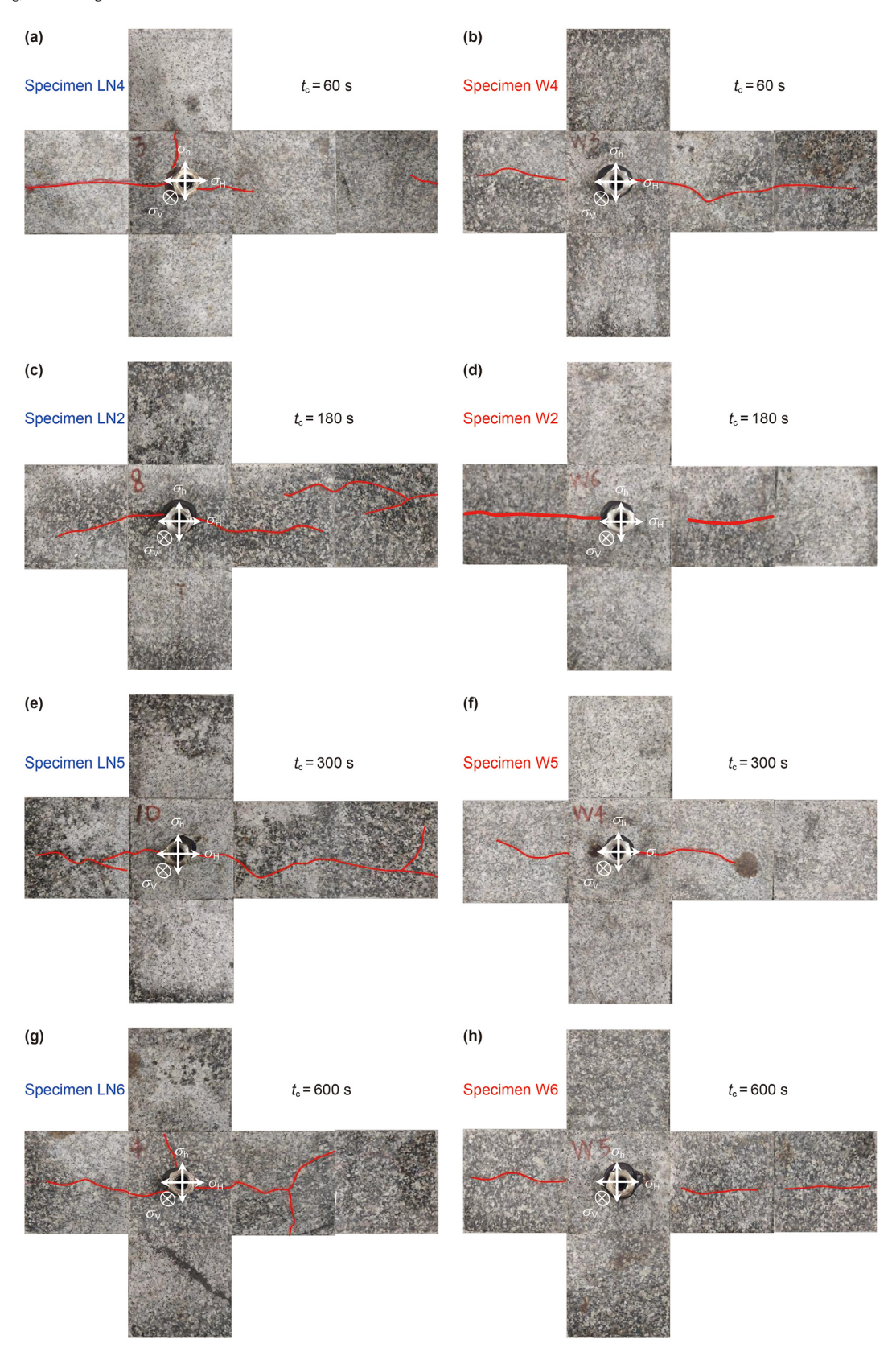


**Fig. 9.** Fracture patterns induced by cyclic LN<sub>2</sub> fracturing ( $\mathbf{a}$ ,  $\mathbf{c}$ ,  $\mathbf{e}$ ) and cyclic water fracturing ( $\mathbf{b}$ ,  $\mathbf{d}$ ,  $\mathbf{f}$ ) under various cooling treatment times  $t_c$ . Red solid lines show the induced fractures.

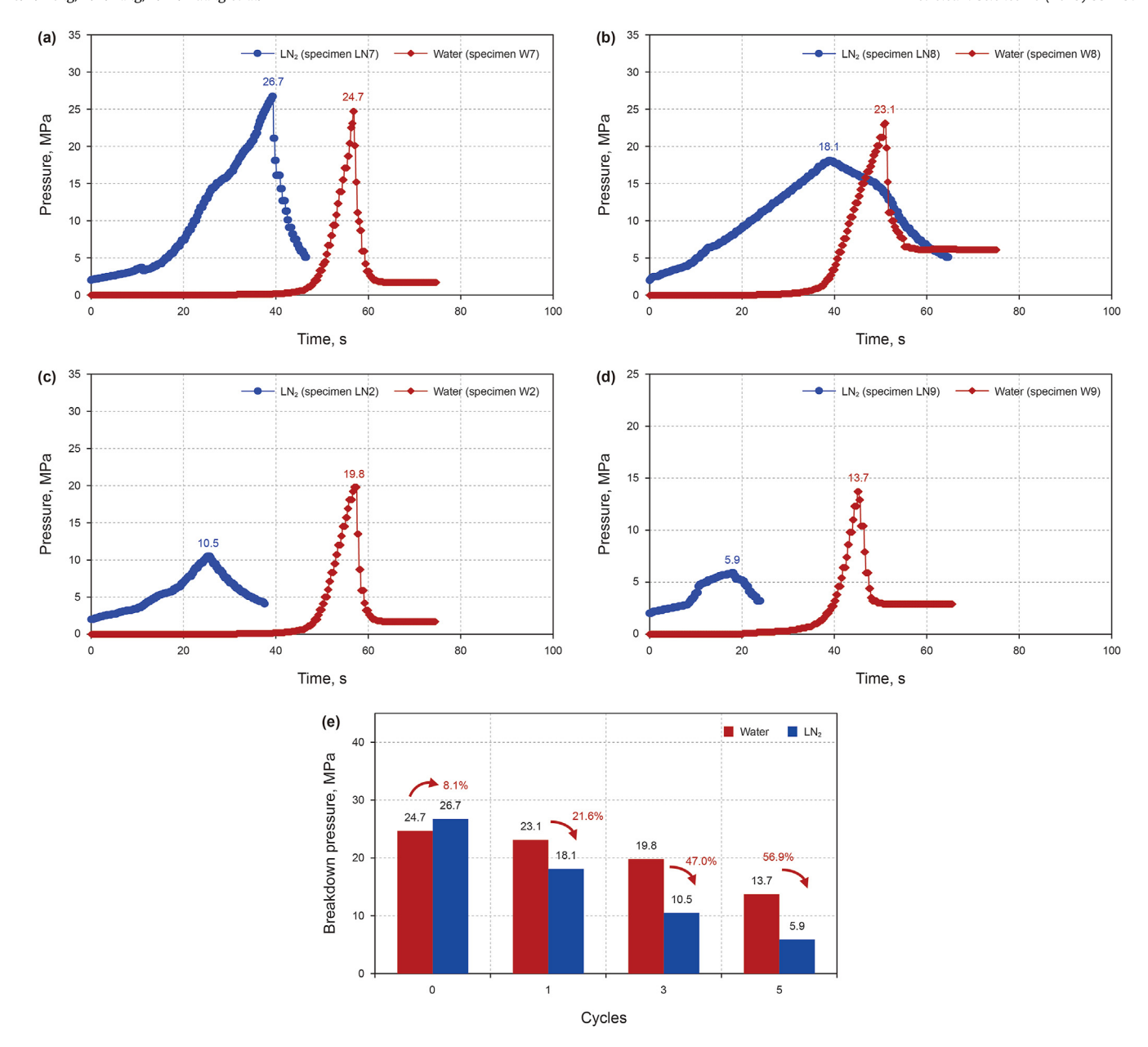


Fig. 10. Pressure—time curves under various number of cycles n: (a) n=0, (b), (c) n=3, and (d) n=5; (e) Comparison of breakdown pressure between cyclic LN<sub>2</sub> fracturing and cyclic water fracturing under various number of cycles. Other experimental parameters are as follows: the cooling treatment pressure  $P_c$  is 2 MPa, cooling treatment time  $t_c$  is 180 s.

It can be found that cyclic LN<sub>2</sub> fracturing can create complex fractures with more micro-fractures and branches compared with cyclic water fracturing. Because they are branched, the fractures tend to have a wider spread than the fractures induced by cyclic water injection, although some are shorter. Besides, the major fractures all extend along the direction of maximum horizontal stress generally. However, the major fractures tend to deviate from the direction of maximum horizontal stress with the increase in the number of cycles by cyclic LN<sub>2</sub> fracturing. It indicated that thermally-induced fractures (not easily controlled by *in-situ* stress) have an important influence on the fracture propagation path. Hence, cyclic LN<sub>2</sub> fracturing has the potential to lead to 3D volumetric patterns that consist of major fractures and branched fractures while cyclic water fracturing can only lead to a bi-wing fracture along with the direction of maximum horizontal stress.

To estimate the fracturing performance under various

conditions quantitatively, the fracture parameters including aperture, length, tortuosity, deviation angle, surface area, and volume of induced fractures were obtained based on 2D CT images and 3D reconstruction as shown in Fig. 13. The calculation method can be seen in Section 2.5. It can be found that the average aperture has a tiny difference in average aperture between cyclic LN2 fracturing and cyclic water fracturing. However, the total length, average tortuosity, total surface area, total volume and average fracture conductivity by cyclic LN<sub>2</sub> fracturing were presented as 210.8%, 19.6%, 143.6%, 142.6% and 773.6% larger than cyclic water fracturing, respectively. Besides, the average aperture, total length, average tortuosity, total surface area and total volume by cyclic LN<sub>2</sub> fracturing were enhanced by 15.0%, 72.72%, 48.1%, 266.6% and 308.7% when the number of cycles increases from 3 to 5, respectively. According to Fig. 13f, the percent of the deviation angle around 0-50° by cyclic LN<sub>2</sub> fracturing was larger than cyclic water

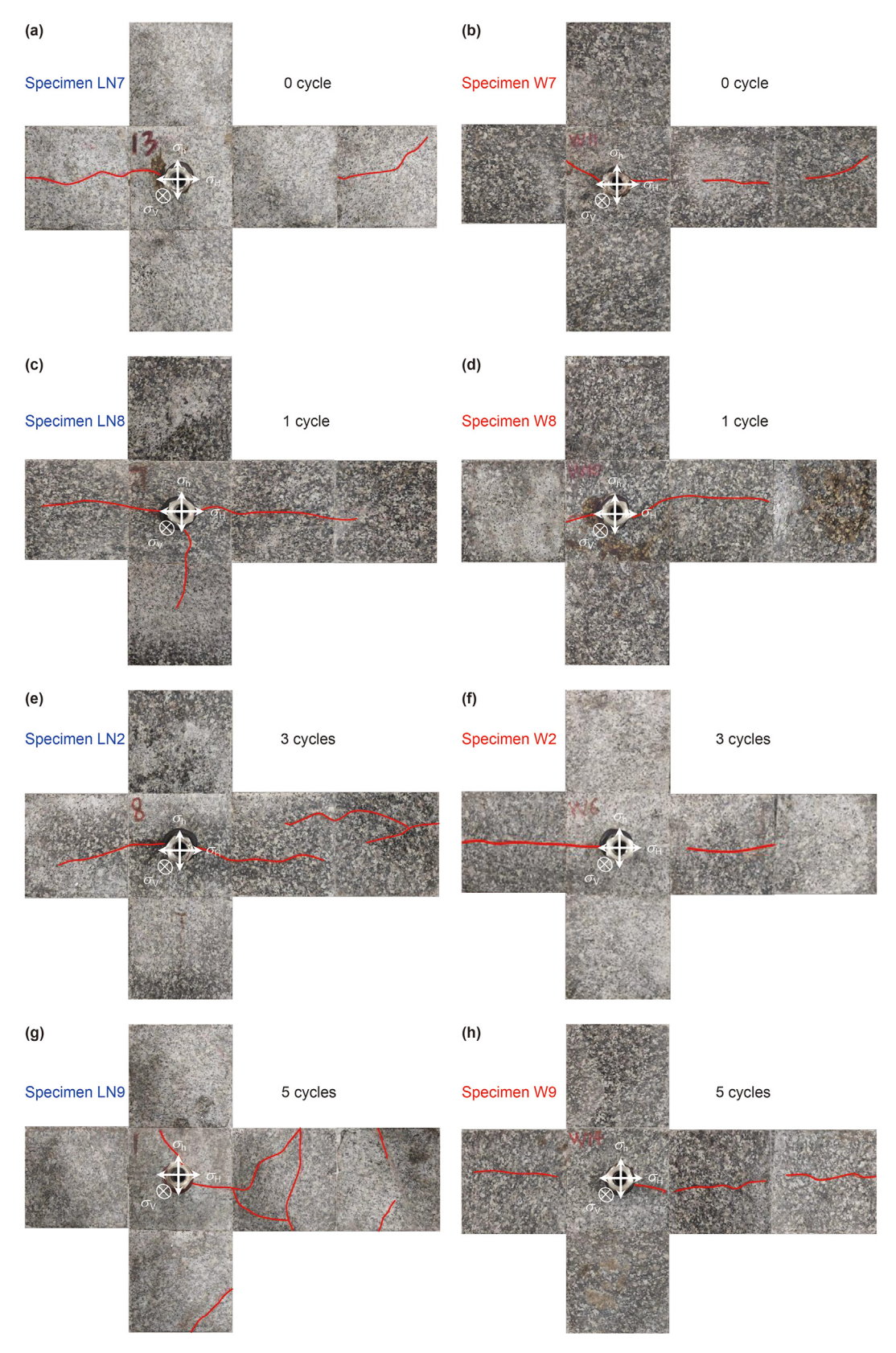


Fig. 11. Fracture patterns induced by cyclic  $LN_2$  fracturing (a, c, e) and cyclic water fracturing (b, d, f) under various cycles. Red solid lines show the induced fractures.

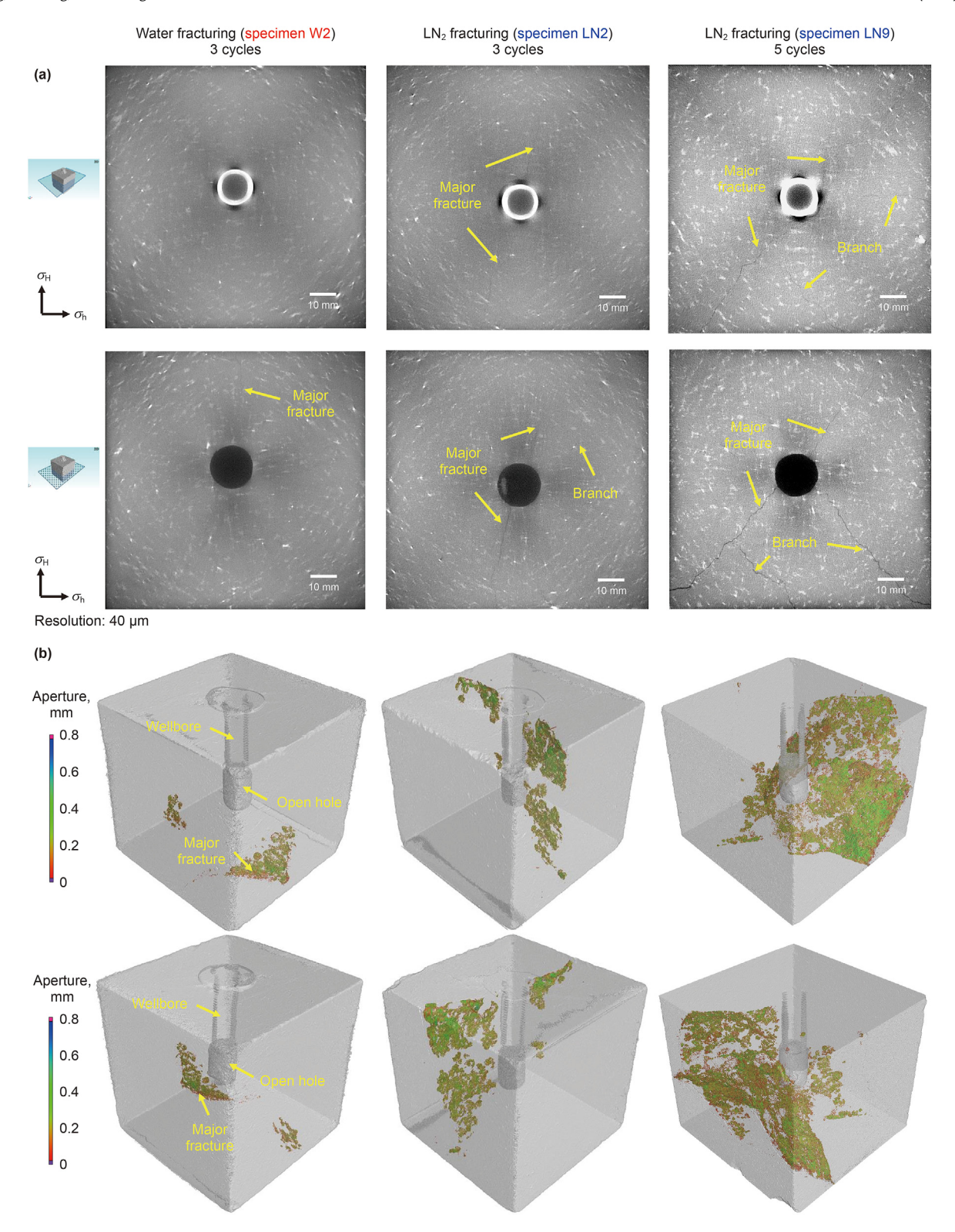


Fig. 12. CT scanning results for specimens W1, LN1 and LN9. (a) X-ray CT 2D slices in horizontal cross-section; (b) 3D reconstructed-fracture-networks.

fracturing. It further indicated that the induced fractures of cyclic  ${\rm LN}_2$  fracturing can be more curved.

In summary, the fracturing performance of cyclic  $LN_2$  fracturing was significantly better than cyclic water fracturing, which is conducive to enhancing the heat exchange efficiency of EGS. Besides, it can be enhanced by increasing the number of cycles.

## 4. Discussion

## 4.1. Cryo-SEM imaging

To make a comparison with the state after  $\text{LN}_2$  cooling treatment, the surface morphology and mineral distribution were first

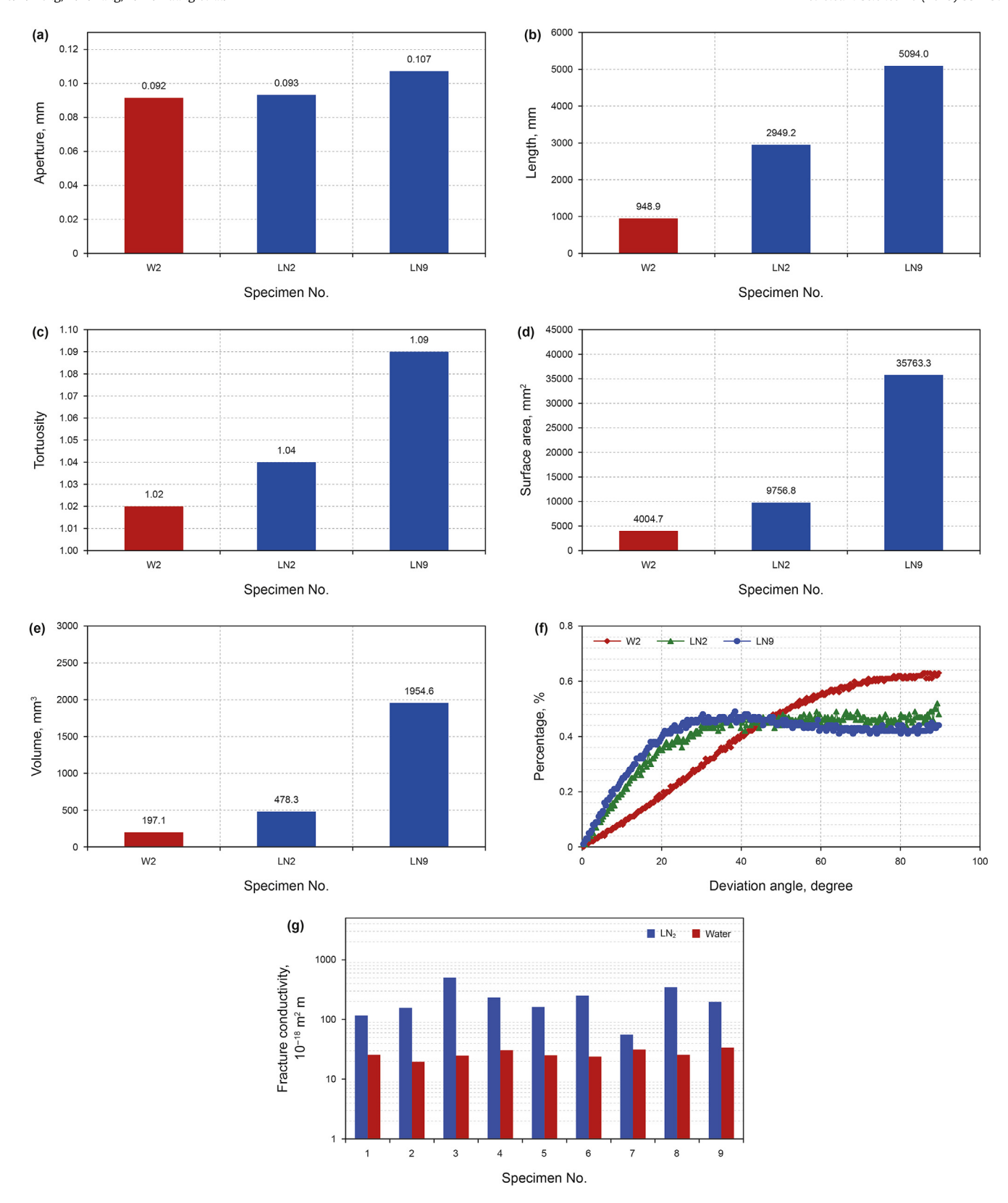


Fig. 13. Comparison of fracture parameters between cyclic LN<sub>2</sub> fracturing and cyclic water fracturing. (a) Average aperture; (b) Total surface area; (c) Average tortuosity of the induced fractures; (d) Total surface area; (e) Total volumes; (f) Deviation angle ratio; (e) Fracture conductivity.

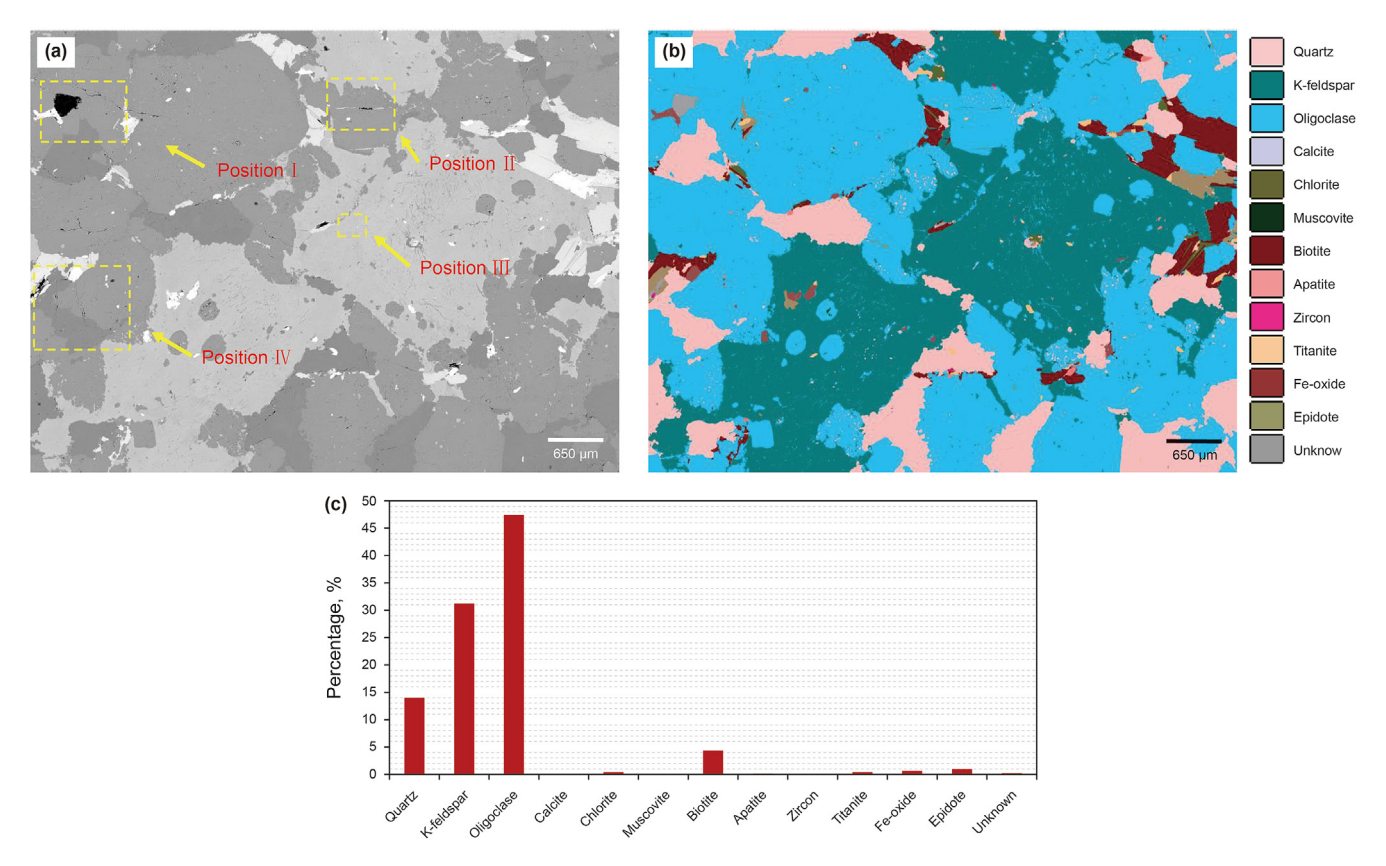


Fig. 14. Standard SEM image analysis. (a) Overall images; (b) Mineral analysis; (c) Mineral contents.

**Table 3**The uniaxial thermal expansion coefficient of main minerals (Chon et al., 2003; Igarashi et al., 2015).

Mineral	K-feldspar	Oligoclase	Quartz	Biotite
Uniaxial thermal expansion coefficient, $10^{-6}  \text{K}^{-1}$	2.0-5.1	5.2-6.0	15.0-24.3	4.44-16.5

measured by using a mineral analysis system as shown in Fig. 14. It can be found that the main minerals in this granite specimen are oligoclase, K-feldspar and quartz, accounting for 47.34%, 32.25% and 14.16% of the total mineral content, respectively. The uniaxial thermal expansion coefficient of main minerals including K-feldspar, oligoclase, quartz and biotite is shown in Table 3. In addition, four representative regions of different minerals were selected for observation. Position I and Position IV were selected around the interfaces of oligoclase and quartz. Position II and Position III were selected inside oligoclase and K-feldspar, respectively.

Figs. 15–18 presented the surface morphological alterations under various cycles at cryogenic *in-situ* conditions in Position I, Position II, Position III and Position IV, respectively. Prior to the LN<sub>2</sub> treatment (0 cycle), several pores with nano to micro sizes existed, but there were no noticeable fractures at the surface. After LN<sub>2</sub> treatment (1 cycle), fractures were initiated with branches in Position I and Position IV. As the number of cycles increased to 3 and 5, the thermally-induced fractures seemed to become more obvious in Position I and Position IV. To compare the change of fracture aperture with the number of cycles, Zoom region I and Zoom region II in Fig. 18 were selected for observation at greater magnification (Fig. 18a and b). It can be found that the fracture width increased with the increment of cycles. The average fracture widths in Fig. 18a were around 2.396, 2.965, and 3.535  $\mu$ m when the number of cycles was 1, 3 and 5, respectively. The average fracture

widths in Fig. 18b were around 5.495, 6.698, and 7.380  $\mu m$  when the numbers of cycles were 1, 3 and 5, respectively. During the period of cyclic LN<sub>2</sub> cooling treatment, some new micro-fractures will be formed as shown in Fig. 19c. Hence, the more cycles, the more complex and wider micro-fractures will be induced, which contribute to enhancing the fracturing performance of LN<sub>2</sub> injection.

Besides, there were still no noticeable fractures at the surface in Position II, Position III as the numbers of cycles were increased to 1, 3 or 5. The main reason is that different minerals have various thermophysical properties (Igarashi et al., 2015). Thus, different minerals expand or extract differently when subjected to thermal shock due to the various thermal expansion coefficients. The unequal expansion or extraction has the potential to lead to deformation mismatch and create sharp thermal shock at mineral boundaries. During LN2 cooling treatment or unloading, stressconcentration points arise at sharp corners between different particles (Zang, 1993). Hence, cementation between adjacent minerals can be easily broken and many intergranular micro-fractures create during this period. However, the intragranular micro-fractures cannot be easily formed. In sum, increasing the number of cycles may be a better choice when it is difficult to increase the cooling rate or there is little effect to prolonging the cooling treatment time.

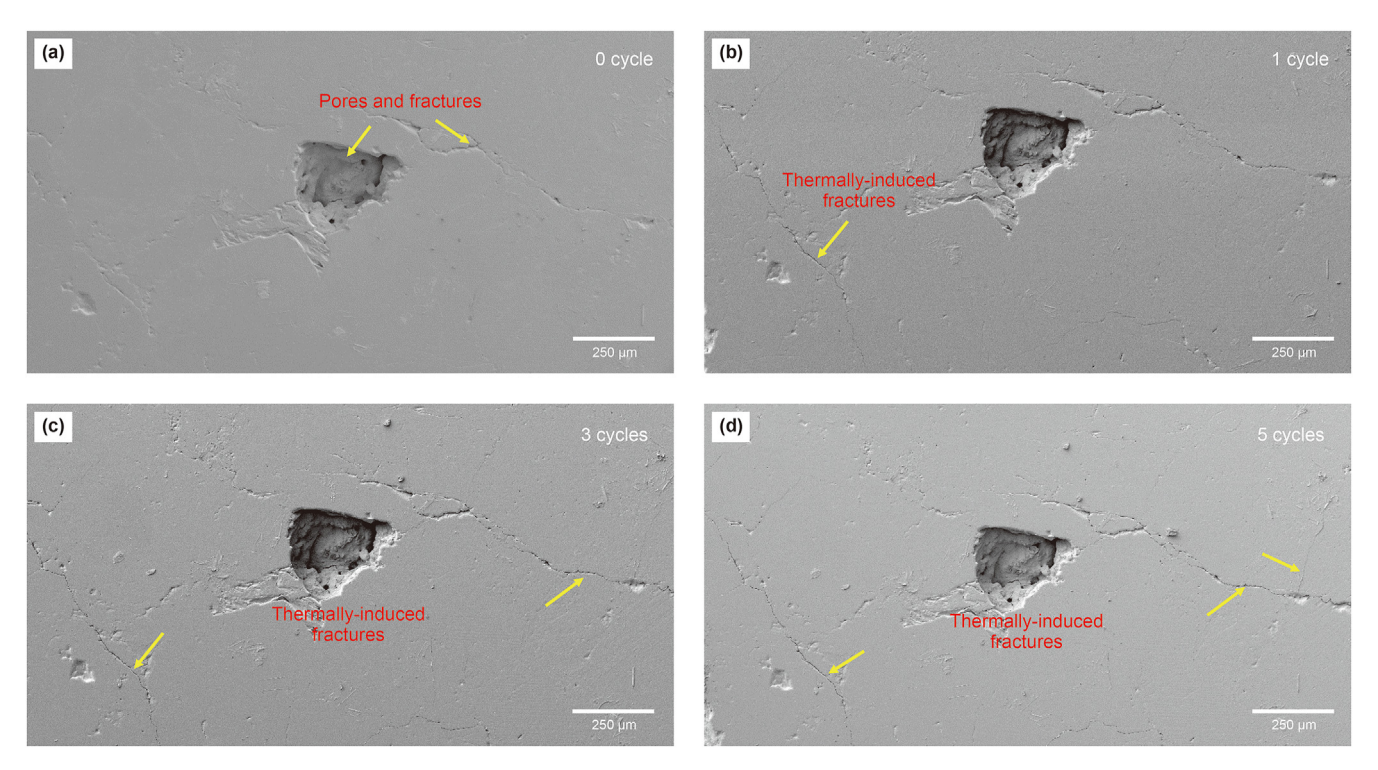


**Fig. 15.** Fracture morphology under various cycles at cryogenic *in-situ* conditions in position I (Fig. 14). (a) Standard SEM image under 0 cycle; (b) Cryo-SEM image under 1 cycle; (c) Cryo-SEM image under 3 cycles; (d) Cryo-SEM image under 5 cycles.

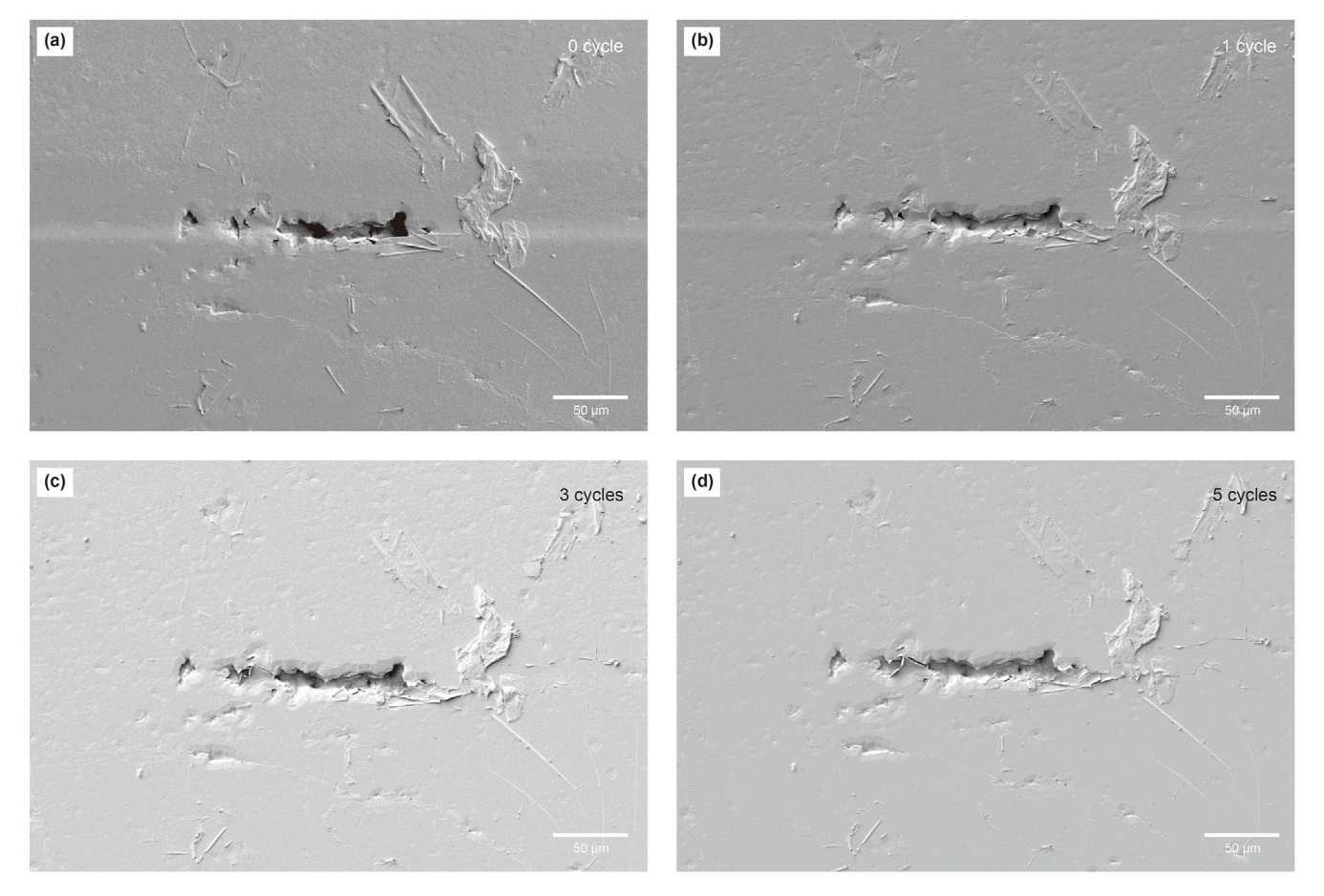


**Fig. 16.** Fracture morphology under various cycles at cryogenic *in-situ* conditions in position II (Fig. 14). (a) Standard SEM image under 0 cycle; (b) Cryo-SEM image under 1 cycle; (c) Cryo-SEM image under 3 cycles; (d) Cryo-SEM image under 5 cycles.

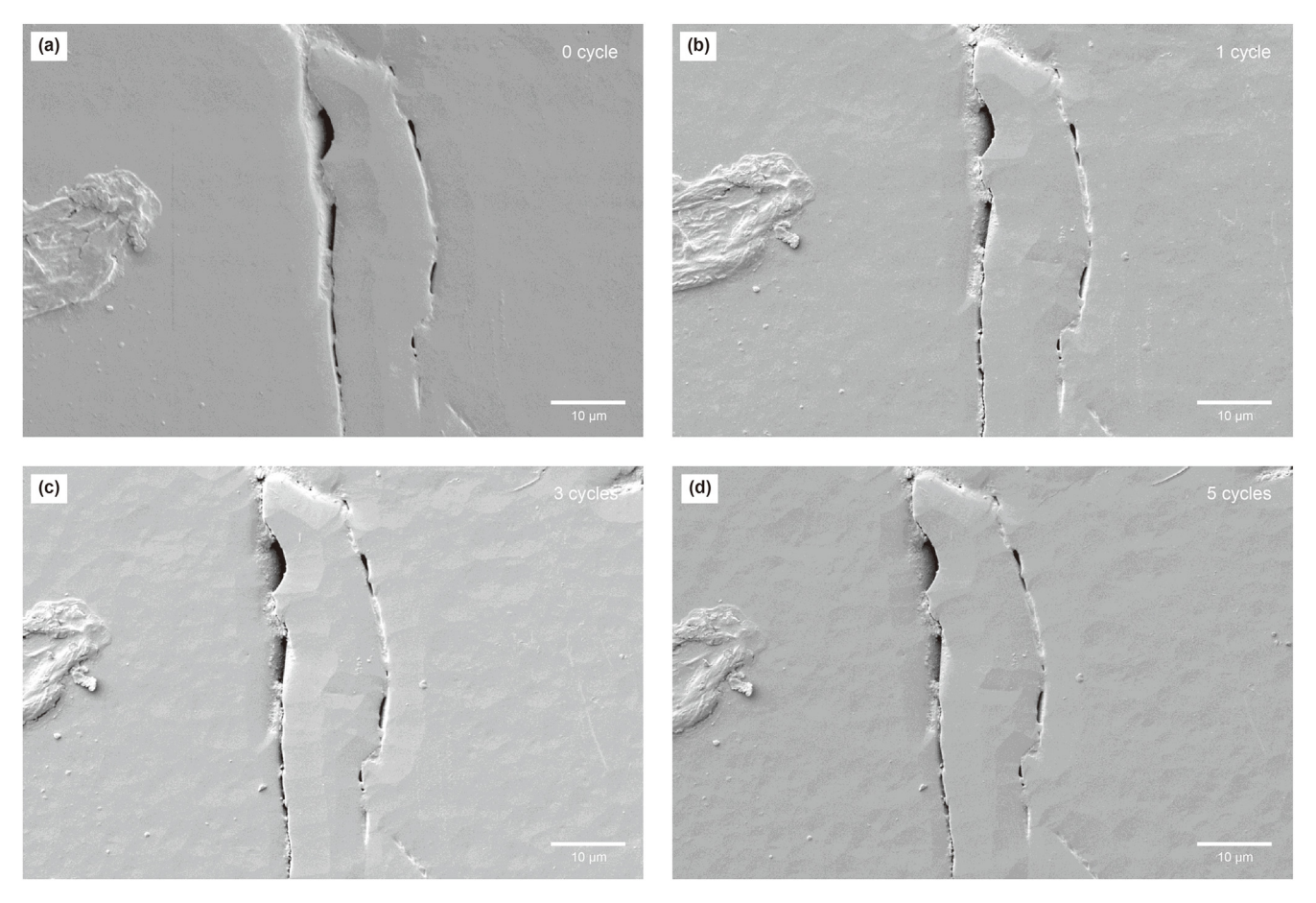


Fig. 17. Fracture morphology under various cycles at cryogenic *in-situ* conditions in position III (Fig. 14). (a) Standard SEM image under 0 cycle; (b) Cryo-SEM image under 1 cycle; (c) Cryo-SEM image under 3 cycles; (d) Cryo-SEM image under 5 cycles.

## 4.2. Field applications

To sum up, LN<sub>2</sub> fracturing performance on HDR can be enhanced by cyclic injection and shows enormous potential to enhance the heat transfer efficiency in EGS. However, the field application of cyclic LN2 fracturing is not easy. A higher cooling rate and huge temperature difference between super-cold LN2 and hightemperature reservoirs are favorable for thermal shock and enhance the thermal shock because it creates larger local thermal gradients. To enhance the efficiency of cyclic LN<sub>2</sub> fracturing, some necessary methods must be taken to ensure LN2 is at a super-cold state during the cyclic injection. For example, the wellheads and pipelines should be made of materials that can withstand the super-cold and high-pressure LN<sub>2</sub> during the cyclic LN<sub>2</sub> fracturing process. The pipelines and boreholes should take pre-cooled treatment by injecting LN<sub>2</sub> at low-pressure levels before injecting high-pressure LN2 into the borehole. In addition, LN2 can be transported through a double-layered tubing with a vacuum annulus (Yang et al., 2019b) or using the heat preservation materials such as fiberglass (McDaniel et al., 1997) to provide a heat transfer barrier during the super-cold LN<sub>2</sub> delivery through the tubing to the high-temperature reservoirs as shown in Fig. 20. Finally, LN<sub>2</sub> is pumped into the reservoirs in a cyclic manner, i.e. alternate high-injection-rate and low-injection-rate. By injecting the cryogenic fracturing fluid in either cyclic injection rate or cyclic injection pressure scheme in HDR formation, rocks will be subjected to cyclic cooling and fatigue failure, which is expected to further lower the breakdown pressure and enhance the stimulated reservoir volume (SRV).

#### 5. Conclusions

In this paper, we proposed an innovative geothermal reservoir stimulation method— cyclic LN<sub>2</sub> fracturing. To verify the efficiency of the method, we conducted cyclic LN<sub>2</sub> fracturing laboratory experiments on granite and compared them with cyclic water fracturing. The breakdown pressures and fracture morphology were investigated under various testing conditions. The effects of cooling treatment time, cooling treatment pressure/rate and number of cycles were analyzed. Then, the fracture parameters in terms of conductivity, aperture, length, tortuosity, deflection angle, surface area and volumes were quantitatively analyzed by using CT scanning. Finally, the fracture morphology on granite specimens induced by cyclic LN<sub>2</sub> treatment under cryogenic conditions was achieved by Cryo-SEM. The following major conclusions were drawn:

(1) Cyclic LN<sub>2</sub> fracturing shows the potential to decrease the breakdown pressure, with 21.3%–67.2% lower pressure in comparison to cyclic water fracturing, but presented 8.1% higher without cooling treatment. Cyclic LN<sub>2</sub> fracturing tends to produce complex and branched fractures, whereas cyclic water fracturing usually produces a single main fracture under a low number of cycles and pressure levels. The total length, average tortuosity, total surface area, total volume and average fracture conductivity can be significantly

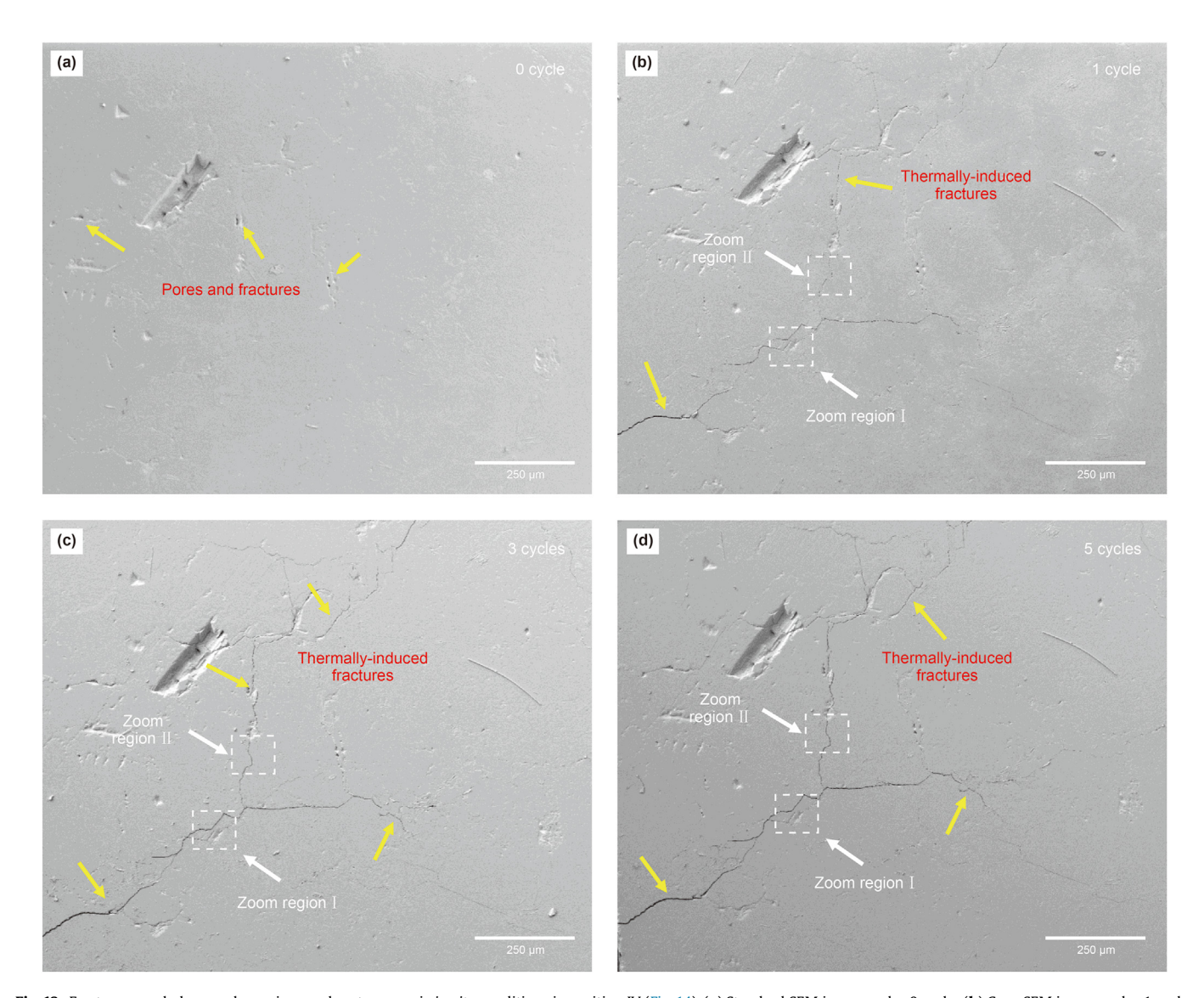


**Fig. 18.** Fracture morphology under various cycles at cryogenic *in-situ* conditions in position IV (Fig. 14). (a) Standard SEM image under 0 cycle; (b) Cryo-SEM image under 1 cycle; (c) Cryo-SEM image under 3 cycles; (d) Cryo-SEM image under 5 cycles.

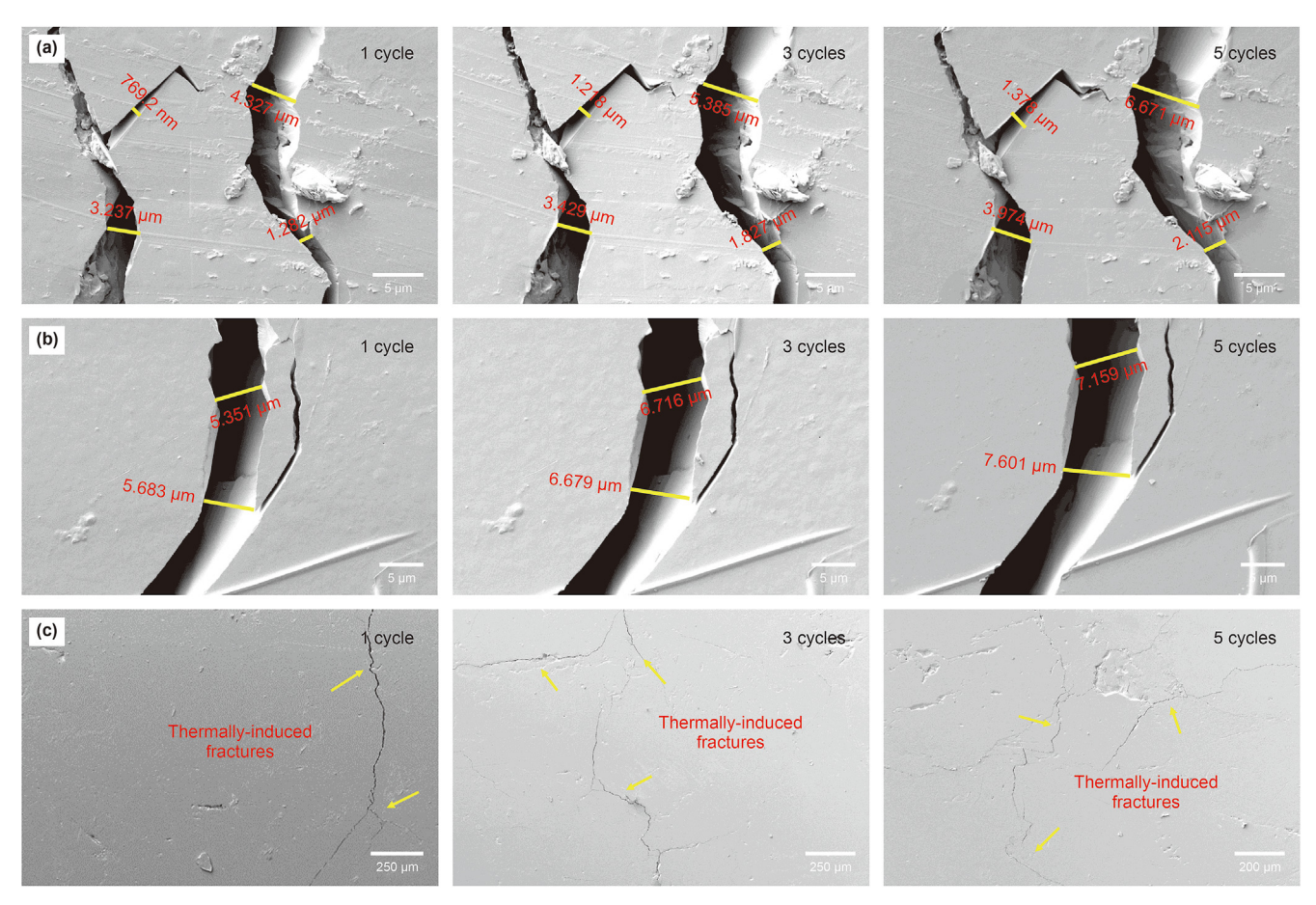
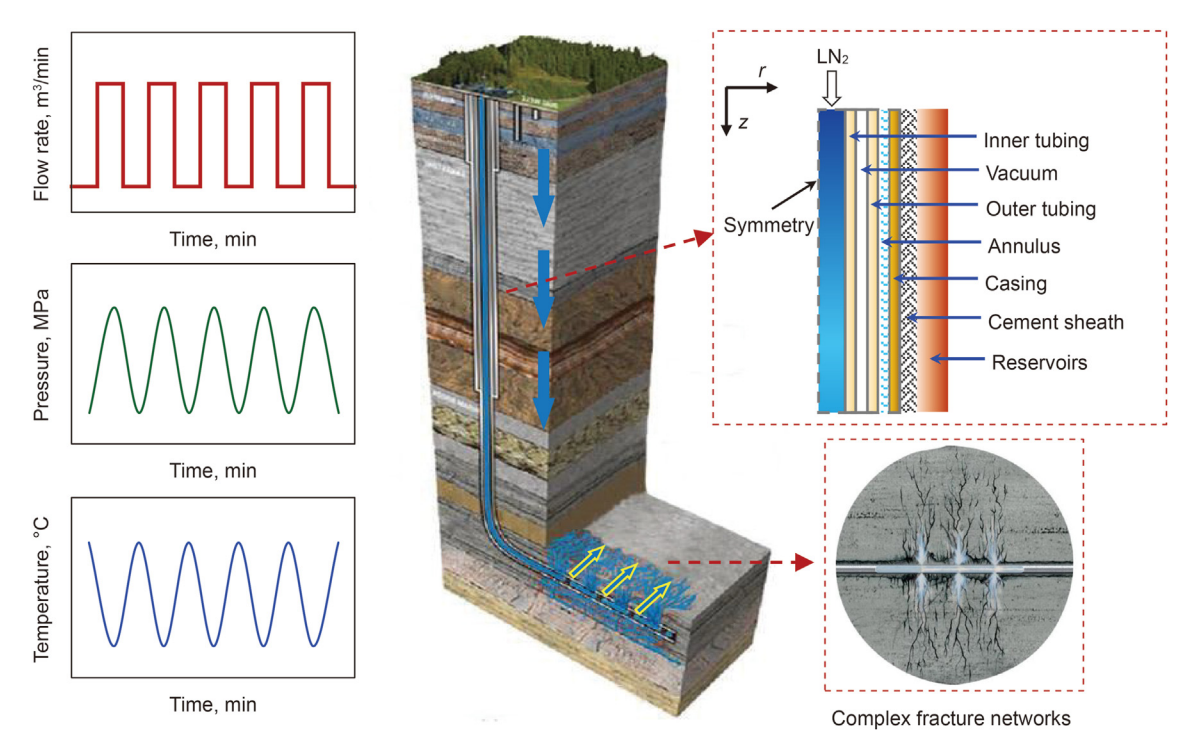


Fig. 19. Fracture morphology under various cycles at cryogenic in-situ conditions. (a) Zoom region I in Fig. 18; (b) Zoom region II in Fig. 18; (c) Cryo-SEM images under various cycles.



 $\textbf{Fig. 20.} \ \ \textbf{Schematic diagram of cyclic LN}_2 \ \ \textbf{fracturing in an HDR reservoir}.$ 

- enhanced by 210.8%, 19.6%, 143.6%, 142.6% and 773.6%, respectively.
- (2) The fracture width increased with the increase in the number of cycles and thermally-induced fractures mostly occur around the interfaces of different particles based on Cryo-SEM and mineral analysis systems. Besides, the average aperture, total length, average tortuosity, total surface area and total volume by cyclic LN<sub>2</sub> fracturing can be enhanced by 15.0%, 72.72%, 48.1%, 266.6% and 308.7% when the number of cycles increases from 3 to 5, respectively.
- (3) Increasing the cooling treatment pressure, cooling treatment time and the number of cycles can improve the complexity of induced fractures and reduce the breakdown pressure. Increasing the number of cycles may be a better choice when it is difficult to increase the cooling rate or there is no significant effect to prolong the cooling treatment time. However, the stimulation performance and engineering cost should be considered together to optimize the number of cycles in the field application.
- (4) The conclusions above are limited to laboratory experiments. The LN<sub>2</sub> fracturing performance by cyclic injection should be further verified through more field applications and numerical studies in the futures.

#### Acknowledgments

This research was supported by the Youth Program of the National Natural Science Foundation of China (52004299), Major Project of the National Natural Science Foundation of China (52192621), the National Science Foundation for National R&D Program for Major Research Instruments of China (51827804), Beijing Outstanding Young Scientist Program (BJJWZYJH01201911414038) and the National Science Foundation for Distinguished Young Scholars of China (51725404). The authors also would like to thank Peking University for our Cryo-SEM work and the Yinghua Inspection and Testing (Shanghai) Co., Ltd for their help in CT scanning and data collection.

## References

- Baisch, S., Weidler, R., Vrs, R., Wyborn, D., Graaf, L.D., 2006. Induced seismicity during the stimulation of a geothermal HFR reservoir in the Cooper Basin, Australia. Bull. Seismol. Soc. Am. 96 (6), 2242–2256. https://doi.org/10.1785/ 0120050255.
- Cha, M., Yin, X., Kneafsey, T., Johanson, B., Alqahtani, N., Miskimins, J., Patterson, T., Wu, Y.S., 2014. Cryogenic fracturing for reservoir stimulation – laboratory studies. J. Petrol. Sci. Eng. 124, 436–450. https://doi.org/10.1016/ j.petrol.2014.09.003.
- Cha, M., Alqahtani, N.B., Yin, X., Kneafsey, T.J., Yao, B., Wu, Y.S., 2017. Laboratory system for studying cryogenic thermal rock fracturing for well stimulation.
   J. Petrol. Sci. Eng. 156, 780–789. https://doi.org/10.1016/j.petrol.2017.06.062.
   Cha, M., Alqahtani, N.B., Yao, B., Yin, X., Kneafsey, T.J., Wang, L., Wu, Y.,
- Cha, M., Alqahtani, N.B., Yao, B., Yin, X., Kneafsey, T.J., Wang, L., Wu, Y., Miskimins, J.L., 2018. Cryogenic fracturing of wellbores under true triaxialconfining stresses: experimental investigation. SPE J. 23 (4), 1271–1289. https://doi.org/10.2118/180071-PA.
- Cha, M., Alqahtani, N.B., Yin, X., Wang, L., Yao, B., Kneafsey, T.J., Miskimins, J.L., Wu, Y.-S., 2021. Propagation of cryogenic thermal fractures from unconfined PMMA boreholes. Energies 14 (17), 5433. https://doi.org/10.3390/en14175433.
- Chon, C.M., Kim, S.A., Moon, H.S., 2003. Crystal structures of biotite at high temperatures and of heat-treated biotite using neutron powder diffraction. Clay Clay Miner. 51 (5), 519–528. https://doi.org/10.1346/ccmn.2003.0510506.
- Deichmann, N., Giardini, D.J.S.R.L., 2009. Earthquakes induced by the stimulation of an enhanced geothermal system below Basel (Switzerland). Seismol Res. Lett. 80 (5), 784–798. https://doi.org/10.1785/gssrl.80.5.784.
- Egert, R., Korzani, M.G., Held, S., Kohl, T., 2020. Implications on large-scale flow of the fractured EGS reservoir Soultz inferred from hydraulic data and tracer experiments. Geothermics 84. https://doi.org/10.1016/j.geothermics.2019.101749.
- EGI, 2018. Frontier Observatory for Research in Geothermal Energy Milford Site, Utah - Phase 2B Final Topical Report. University of Utah, Salt Lake City.
- EPA, 2016. Hydraulic Fracturing for Oil and Gas: Impacts from the Hydraulic Fracturing Water Cycle on Drinking Water Resources in the United States, Office of Research and Development. U.S. Environmental Protection Agency,

#### Washington, D.C.

- Feng, G., Wang, X., Kang, Y., Zhang, Z., 2020. Effect of thermal cycling-dependent cracks on physical and mechanical properties of granite for enhanced geothermal system. Int. J. Rock Mech. Min. Sci. 134, 104476. https://doi.org/ 10.1016/j.ijrmms.2020.104476.
- Hofmann, H., Babadagli, T., Zimmermann, G., 2014. Hot water generation for oil sands processing from enhanced geothermal systems: process simulation for different hydraulic fracturing scenarios. Appl. Energy 113, 524–547. https:// doi.org/10.1016/j.apenergy.2013.07.060.
- Hofmann, H., Zimmermann, G., Zang, A., Min, K.B., 2018. Cyclic soft stimulation (CSS): a new fluid injection protocol and traffic light system to mitigate seismic risks of hydraulic stimulation treatments. Geoth. Energy 6 (1), 1–33. https://doi.org/10.1186/s40517-018-0114-3.
- Hong, C., Yang, R., Huang, Z., Qin, X., Wen, H., Cong, R., Liu, W., Chen, J., 2022. Fracture initiation and morphology of tight sandstone by liquid nitrogen fracturing. Rock Mech. Rock Eng. 55, 1285–1301. https://doi.org/10.1007/s00603-021-02755-x.
- Hou, P., Gao, F., Gao, Y., Yang, Y., Cai, C., 2018. Changes in breakdown pressure and fracture morphology of sandstone induced by nitrogen gas fracturing with different pore pressure distributions. Int. J. Rock Mech. Min. Sci. 109, 84–90. https://doi.org/10.1016/j.ijrmms.2018.06.006.
  Huang, P., Huang, Z., Yang, Z., Wu, X., Li, R., Zhang, S., 2019. An innovative experi-
- Huang, P., Huang, Z., Yang, Z., Wu, X., Li, R., Zhang, S., 2019. An innovative experimental equipment for liquid nitrogen fracturing. Rev. Sci. Instrum. 90 (3), 036104. https://doi.org/10.1063/1.5086448.
- Huang, Z., Zhang, S., Yang, R., Wu, X., Li, R., Zhang, H., Hung, P., 2020. A review of liquid nitrogen fracturing technology. Fuel 266, 117040. https://doi.org/10.1016/ j.fuel.2020.117040.
- Igarashi, G., Maruyama, I., Nishioka, Y., Yoshida, H., 2015. Influence of mineral composition of siliceous rock on its volume change. Construct. Build. Mater. 94, 701–709. https://doi.org/10.1016/j.conbuildmat.2015.07.071.
- Kelkar, S., WoldeGabriel, G., Rehfeldt, K., 2016. Lessons learned from the pioneering hot dry rock project at Fenton Hill, USA. Geothermics 63, 5–14. https://doi.org/10.1016/j.geothermics.2015.08.008.
- Kim, K.-I., Min, K.-B., Kim, K.-Y., Choi, J.W., Yoon, K.-S., Yoon, W.S., Yoon, B., Lee, T.J., Song, Y., 2018. Protocol for induced microseismicity in the first enhanced geothermal systems project in Pohang, Korea. Renew. Sustain. Energy Rev. 91, 1182–1191. https://doi.org/10.1016/j.rser.2018.04.062.
- Lei, Z., Zhang, Y., Yu, Z., Hu, Z., Li, L., Zhang, S., Fu, L., Zhou, L., Xie, Y., 2019. Exploratory research into the enhanced geothermal system power generation project: the Qiabuqia geothermal field, Northwest China. Renew. Energy 139, 52–70. https://doi.org/10.1016/j.renene.2019.01.088.
- Li, M.H., Zhou, F.J., Liu, J.J., Yuan, L.S., Huang, G.P., Wang, B., 2022. Quantitative investigation of multi-fracture morphology during TPDF through true tri-axial fracturing experiments and CT scanning. Petrol. Sci. 19 (4), 1700–1717. https://doi.org/10.1016/j.petsci.2022.03.017.
- Li, Q., Li, X., Yin, T., 2021. Factors affecting pore structure of granite under cyclic heating and cooling: a nuclear magnetic resonance investigation. Geothermics 96, 102198. https://doi.org/10.1016/j.geothermics.2021.102198.
- Li, R., Huang, Z., Wu, X., Yan, P., Dai, X., 2018. Cryogenic quenching of rock using liquid nitrogen as a coolant: investigation of surface effects. Int. J. Heat Mass Tran. 119, 446–459. https://doi.org/10.1016/j.ijheatmasstransfer.2017.11.123.
- Li, R., Wu, X., Huang, Z., 2019. Jet impingement boiling heat transfer from rock to liquid nitrogen during cryogenic quenching. Exp. Therm. Fluid Sci. 106, 255–264. https://doi.org/10.1016/j.expthermflusci.2019.04.016.
- Lu, S.M., 2018. A global review of enhanced geothermal system (EGS). Renew. Sustain. Energy Rev. 81, 2902–2921. https://doi.org/10.1016/j.rser.2017.06.097.
- Lv, Y., Yuan, C., Zhu, X., Gan, Q., Li, H., 2022. THMD analysis of fluid injection-induced fault reactivation and slip in EGS. Geothermics 99, 102303. https://doi.org/10.1016/j.geothermics.2021.102303.
- McDaniel, B., Grundmann, S.R., Kendrick, W.D., Wilson, D.R., Jordan, S.W., 1997. Field applications of cryogenic nitrogen as a hydraulic fracturing fluid. SPE Annual Technical Conference and Exhibition. https://doi.org/10.2118/38623-MS.
- Pai, N., Feng, J., Haijian, S., Zequan, H., Meng, X., Yazhen, Z., Cheng, Z., Dong, W., 2021. An investigation on the deterioration of physical and mechanical properties of granite after cyclic thermal shock. Geothermics 97, 102252. https:// doi.org/10.1016/j.geothermics.2021.102252.
- Park, S., Xie, L., Kim, K.I., Kwon, S., Min, K.B., Choi, J., Yoon, W.S., Song, Y., 2017. First hydraulic stimulation in fractured geothermal reservoir in Pohang PX-2 Well. Procedia Eng. 191, 829–837. https://doi.org/10.1016/j.proeng.2017.05.250.
- Patel, S.M., Sondergeld, C.H., Rai, C.S., 2017. Laboratory studies of hydraulic fracturing by cyclic injection. Int. J. Rock Mech. Min. Sci. 95, 8–15. https://doi.org/10.1016/j.ijrmms.2017.03.008.
- Rahimi-Aghdam, S., Chau, V.T., Lee, H., Nguyen, H., Li, W., Karra, S., Rougier, E., Viswanathan, H., Srinivasan, G., Bažant, Z.P., 2019. Branching of hydraulic cracks enabling permeability of gas or oil shale with closed natural fractures. Proc. Natl. Acad. Sci. USA 116 (5), 1532–1537. https://doi.org/10.1073/pnas.1818529116.
- Rong, G., Sha, S., Li, B., Chen, Z., Zhang, Z., 2021. Experimental investigation on physical and mechanical properties of granite subjected to cyclic heating and liquid nitrogen cooling. Rock Mech. Rock Eng. 54 (5), 2383–2403. https:// doi.org/10.1007/s00603-021-02390-6.
- Song, G., Song, X., Li, G., Shi, Y., Wang, G., Ji, J., Xu, F., Song, Z., 2021. An integrated multi-objective optimization method to improve the performance of multilateral-well geothermal system. Renew. Energy 172, 1233–1249. https:// doi.org/10.1016/j.renene.2021.03.073.

- Sun, Y., Zhai, C., Xu, J., Yu, X., Cong, Y., Zheng, Y., Tang, W., Li, Y., 2022. Damage and failure of hot dry rock under cyclic liquid nitrogen cold shock treatment: a nondestructive ultrasonic test method. Nat. Resour. Res. 31 (1), 261–279. https:// doi.org/10.1007/s11053-021-10005-8.
- Tenma, N., Yamaguchi, T., Zyvoloski, G., 2008. The Hijiori hot dry rock test site, Japan. Geothermics 37 (1), 19–52. https://doi.org/10.1016/j.geothermics.2007.11.002.
- Wang, G., Song, X., Shi, Y., Yang, R., Yulong, F., Zheng, R., Li, J., 2021. Heat extraction analysis of a novel multilateral-well coaxial closed-loop geothermal system. Renew. Energy 163, 974–986. https://doi.org/10.1016/j.renene.2020.08.121.
- Wang, L., Yao, B., Cha, M., Alqahtani, N.B., Patterson, T.W., Kneafsey, T.J., Miskimins, J.L., Yin, X., Wu, Y.-S., 2016. Waterless fracturing technologies for unconventional reservoirs-opportunities for liquid nitrogen. J. Nat. Gas Sci. Eng. 35, 160–174. https://doi.org/10.1016/j.jngse.2016.08.052.
- Wen, H., Yang, R., Huang, Z., Hu, X., Hong, C., Song, G., 2022. Flow and heat transfer of nitrogen during liquid nitrogen fracturing in coalbed methane reservoirs. J. Petrol. Sci. Eng. 209, 109900. https://doi.org/10.1016/j.petrol.2021.109900.
- Wu, X., Huang, Z., Cheng, Z., Zhang, S., Song, H., Zhao, X., 2019. Effects of cyclic heating and LN<sub>2</sub>-cooling on the physical and mechanical properties of granite. Appl. Therm. Eng. 156, 99–110. https://doi.org/10.1016/i.applthermaleng.2019.04.046.
- Japplthermaleng.2019.04.046.

  Yang, B., Wang, H., Wang, B., Shen, Z., Zheng, Y., Jia, Z., Yan, W., 2021a. Digital quantification of fracture in full-scale rock using micro-CT images: a fracturing experiment with N<sub>2</sub> and CO<sub>2</sub>. J. Petrol. Sci. Eng. 196, 107682. https://doi.org/10.1016/j.petrol.2020.107682.
- Yang, R., Hong, C., Huang, Z., Song, X., Zhang, S., Wen, H., 2019a. Coal breakage using abrasive liquid nitrogen jet and its implications for coalbed methane recovery. Appl. Energy 253, 113485. https://doi.org/10.1016/j.apenergy.2019.113485.
- Yang, R., Huang, Z., Shi, Y., Yang, Z., Huang, P., 2019b. Laboratory investigation on cryogenic fracturing of hot dry rock under triaxial-confining stresses. Geothermics 79, 46–60. https://doi.org/10.1016/j.geothermics.2019.01.008.
- Yang, R., Hong, C., Huang, Z., Wen, H., Li, X., Huang, P., Liu, W., Chen, J., 2021b. Liquid nitrogen fracturing in boreholes under true triaxial stresses: laboratory investigation on fractures initiation and morphology. SPE J. 26 (1), 135–154. https:// doi.org/10.2118/201224-PA.
- Yang, R., Hong, C., Liu, W., Wu, X., Wang, T., Huang, Z., 2021c. Non-contaminating cryogenic fluid access to high-temperature resources: liquid nitrogen fracturing in a lab-scale Enhanced Geothermal System. Renew. Energy 165, 125–138. https://doi.org/10.1016/j.renene.2020.11.006.
- Yoon, C.E., Huang, Y., Ellsworth, W.L., Beroza, G.C., 2017. Seismicity during the initial stages of the Guy-Greenbrier, Arkansas, earthquake sequence. J. Geophys. Res. Solid Earth 122 (11), 9253–9274. https://doi.org/10.1002/2017JB014946.

- Zang, A., 1993. Finite element study on the closure of thermal microcracks in feldspar/quartz-rocks—I. Grain-boundary cracks. Geophys. J. Int. 113 (1), 17–31. https://doi.org/10.1111/j.1365-246X.1993.tb02525.x.
- Zang, A., Yoon, J.S., Stephansson, O., Heidbach, O., 2013. Fatigue hydraulic fracturing by cyclic reservoir treatment enhances permeability and reduces induced seismicity. Geophys. J. Int. 195 (2), 1282–1287. https://doi.org/10.1093/gji/get301.
- Zang, A., Zimmermann, G., Hofmann, H., Stephansson, O., Min, K.B., Kim, K.Y., 2018. How to reduce fluid-injection-induced seismicity. Rock Mech. Rock Eng. 52 (2), 475—493. https://doi.org/10.1007/s00603-018-1467-4.
- Zang, A., Zimmermann, G., Hofmann, H., Niemz, P., Kim, K.Y., Diaz, M., Zhuang, L., Yoon, J.S., 2021. Relaxation damage control via fatigue-hydraulic fracturing in granitic rock as inferred from laboratory-, mine-, and field-scale experiments. Sci. Rep. 11 (1), 6780. https://doi.org/10.1038/s41598-021-86094-5.
- Zhang, W., Qu, Z., Guo, T., Wang, Z., 2019. Study of the enhanced geothermal system (EGS) heat mining from variably fractured hot dry rock under thermal stress. Renew. Energy 143, 855–871. https://doi.org/10.1016/j.renene.2019.05.054.
- Zhang, Y., Zhang, J., Yuan, B., Yin, S., 2018. In-situ stresses controlling hydraulic fracture propagation and fracture breakdown pressure. J. Petrol. Sci. Eng. 164, 164–173. https://doi.org/10.1016/j.petrol.2018.01.050.
- Zhu, Z., Ranjith, P.G., Tian, H., Jiang, G., Dou, B., Mei, G., 2021. Relationships between P-wave velocity and mechanical properties of granite after exposure to different cyclic heating and water cooling treatments. Renew. Energy 168, 375–392. https://doi.org/10.1016/j.renene.2020.12.048.
- Zhuang, L., Kim, K., Jung, S., Diaz, M., Min, K.B., Park, S., Zang, A., Stephansson, O., Zimmerman, G., Yoon, J., 2016. Laboratory study on cyclic hydraulic fracturing of pocheon granite in Korea. 50th US Rock Mechanics/Geomechanics Symposium, ARMA-2016-163
- Zhuang, L., Kim, K.Y., Jung, S.G., Diaz, M., Min, K.B., Zang, A., Stephansson, O., Zimmermann, G., Yoon, J.-S., Hofmann, H., 2019. Cyclic hydraulic fracturing of pocheon granite cores and its impact on breakdown pressure, acoustic emission amplitudes and injectivity. Int. J. Rock Mech. Min. Sci. 122, 104065. https://doi.org/10.1016/j.ijrmms.2019.104065.
- Zhuang, L., Jung, S.G., Diaz, M., Kim, K.Y., Hofmann, H., Min, K.-B., Zang, A., Stephansson, O., Zimmermann, G., Yoon, J.-S., 2020. Laboratory true triaxial hydraulic fracturing of granite under six fluid injection schemes and grain-scale fracture observations. Rock Mech. Rock Eng. 53 (10), 4329–4344. https://doi.org/10.1007/s00603-020-02170-8.
- Zhuang, L., Zang, A., 2021. Laboratory hydraulic fracturing experiments on crystal-line rock for geothermal purposes. Earth Sci. Rev. 216, 103580. https://doi.org/10.1016/j.earscirev.2021.103580.